MIF2 Is Required for Mitotic Spindle Integrity during Anaphase Spindle Elongation in *Saccharomyces cerevisiae*

Megan T. Brown, Loretta Goetsch, and Leland H. Hartwell

Department of Genetics, SK-50, University of Washington, Seattle, Washington 98195

Abstract. The function of the essential *MIF2* gene in the *Saccharomyces cerevisiae* cell cycle was examined by overexpressing or creating a deficit of *MIF2* gene product. When *MIF2* was overexpressed, chromosomes missegregated during mitosis and cells accumulated in the G_2 and M phases of the cell cycle. Temperature sensitive mutants isolated by in vitro mutagenesis delayed cell cycle progression when grown at the restrictive temperature, accumulated as large budded cells that had completed DNA replication but not chromosome segregation, and lost viability as they passed through mitosis. Mutant cells also showed increased levels of mitotic chromosome loss, supersensitivity to the microtubule destabilizing drug MBC, and morphologically aberrant spindles. *mif2* mutant spindles arrested development immediately before anaphase spindle elongation, and then frequently broke apart into two disconnected short half spindles with misoriented spindle pole bodies. These findings indicate that *MIF2* is required for structural integrity of the spindle during anaphase spindle elongation. The deduced Mif2 protein sequence shared no extensive homologies with previously identified proteins but did contain a short region of homology to a motif involved in binding AT rich DNA by the *Drosophila* D1 and mammalian HMGI chromosomal proteins.

CHROMOSOME segregation is a highly accurate process common to all eukaryotic cells. When chromosomes are missegregated during mitosis, the result is aneuploidy and frequently cellular death. Of central importance to successful chromosome segregation is the correct functioning of the segregation machinery, the spindle apparatus (for review see McIntosh and Koonce, 1989). Spindles are composed of two sets of interdigitating microtubules (half spindles) that originate at the spindle poles. The minus ends of the spindle microtubules are located at the poles and the plus ends in the spindle midzone, forming an antiparallel microtubule array in the region of half spindle overlap. In order for successful chromosome segregation to occur, spindles must form stable associations with chromosomes, and then function in two very different ways during the two substages of anaphase. In anaphase A, the pole to chromosome spindle microtubules (kinetochore microtubules) depolymerize as sister chromatids separate, leave the metaphase plate, and are translocated via their kinetochores along the microtubules toward the spindle poles. In anaphase B, the distance between the poles increases as the spindle microtubules not attached to chromosomes (polar microtubules) elongate, ensuring the complete separation of chromosomes both from their sisters and into separate daughter cells. Elongation is achieved both by a sliding apart of the antiparallel microtubules and by an increase in polar microtubule length via tubulin polymerization (for review see Cande and Hogan, 1989).

S. cerevisiae is an excellent system in which to study the mechanics of chromosome segregation and spindle behavior. Compared to most eukaryotes, *S. cerevisiae* tolerates whole chromosome aneuploidy relatively well and can therefore grow under conditions of low segregational fidelity. Segregation errors can be detected by scoring chromosome specific genetic markers in highly sensitive assays that measure the accuracy of chromosome transmission. The yeast spindle is similar in most respects to the spindle of higher eukaryotes and undergoes a well characterized cycle of development as determined by electron and immunofluorescence microscopy (Byers and Goetsch, 1975; Kilmartin and Adams, 1984). During interphase the yeast spindle pole, called the spindle pole body (SPB)[1], duplicates to generate two side-by-side SPBs embedded in the nuclear envelope, which unlike the nuclear membrane of higher eukaryotes remains intact throughout mitosis. As the cell cycle progresses, the SPBs separate from each other, forming a short spindle between them. The nucleus then migrates to the junction between the mother cell and attached daughter bud, and the spindle elongates. Cytokinesis is accompanied by the break-

Please address all correspondence to Dr. Megan Brown, Fred Hutchinson Cancer Research Center, Division of Basic Sciences, A2-025, 1124 Columbia Street, Seattle, WA 98104.

1. *Abbreviations used in this paper:* C, complete synthetic medium; CAI, Codon Adaptation Index; FACS, fluorescence-activated cell sorter; MBC, methyl benzimidazole-2-yl-carbamate; −N, minimal synthetic medium having no nitrogen source; SPB, spindle pole body.

down of any remaining long spindle microtubules and results in the generation of two daughter nuclei, each with a single SPB and interphase array of microtubules. A variety of mutants have been isolated that identify genes required for spindle development and/or chromosome segregation (Brown et al., 1993).

The mitotic fidelity gene *MIF2* was isolated for its ability to destabilize chromosome VII when overexpressed (Meeks-Wagner et al., 1986) and was shown to be an essential gene by gene disruption. Spores carrying a *MIF2* null allele arrested growth after several divisions as large budded cells, a morphology characteristic of cells blocked in DNA replication or mitosis. These results suggested that *MIF2* has an essential cell cycle function and is potentially involved in mitotic chromosome segregation. To further define the role of *MIF2* in the cell cycle and determine whether it indeed plays a role in chromosome segregation, we isolated temperature sensitive lethal alleles and examined the phenotypes of cells deficient for *MIF2* function. Our results indicate that Mif2 protein is required for maintaining the structural integrity of the mitotic spindle.

Materials and Methods

Strains and Media

All *S. cerevisiae* strains used were of congenic A364a genetic background unless otherwise noted and are listed in Table I. *E. coli* strain JA194 (*trpC-117 leuB rk⁻ mk⁺*) was used to assay plasmid-borne yeast *TRP1* function.

The yeast media used were the two rich media YM-1 (Hartwell, 1967) and YEPD (Sherman et al., 1986), a complete (C) synthetic medium (Sherman et al., 1986), and a minimal synthetic medium lacking a nitrogen source (−N). −N medium consisted of 1.6 g/liter of yeast nitrogen base without amino acids or ammonium sulfate (Difco Labs., Detroit, MI), 0.09 M succinic acid, adjusted to pH 5.8 with NaOH. Rich medium plates were YEPD + 2% Bacto-agar (Difco Labs.). Synthetic plates were C medium with 2% added Bacto-agar. For selection against auxotrophic markers, C medium minus the substance(s) required for growth was used (e.g., C− tryptophan). YEPD + cycloheximide (Sigma Chem. Co., St. Louis, MO) plates contained 10 μg/ml of cycloheximide. Canavanine plates consisted of C−arginine medium containing 60 μg/ml canavanine sulfate (Sigma Chem. Co.). Methyl benzimidazole-2-yl-carbamate (MBC), a gift of Du Pont Corp. (Wilmington, DE), was added to YEPD or C plates at concentrations of 10, 15, 20, and 40 μg/ml. *E. coli* was grown in L Broth and on LB or M9 agar plates.

Plasmid Constructions

pMB001 was constructed by inserting a 4.4-kb *Bam*H I fragment containing the *MIF2* partial gene into the *Bam*H I site of JK007, a CEN3 ARS1 *URA3* vector. JK007 was constructed by J. Konopka by filling in the *Eco*R I and *Hind* III sites of pDK263 (Koshland et al., 1985). pMB002 was constructed by inserting the same 4.4-kb *Bam*H I fragment into the CEN4 ARS1 *URA3* vector YCp50. Plasmid SC231 consists of the 4.4-kb *Bam*H I fragment cloned into the *Bam*H I site of the multiple copy 2 μm *LEU2* vector CV13 (Broach et al., 1979) as described by Meeks-Wagner et al. (1986), who referred to SC231 as YEpSC231. A 2.0 *Bam*H I fragment deriving from chromosome IX is also present in SC231. Plasmid S26 consists of the 4.4-kb *Bam*H I fragment cloned into the *Bam*H I site of the multiple copy ARS1 *TRP1* vector YRp7 (Tschumper and Carbon, 1980) and was referred to as YpSC231-4 by Meeks-Wagner et al. (1986). pMB024 was constructed by inserting a 3.0-kb *Bam*H I fragment containing half of the *MIF2* gene into the *Bam*H I site of pMB017 immediately adjacent to the 4.4-kb *Bam*H I fragment containing the other half of the *MIF2* gene. This juxtaposition reconstructed the intact *MIF2* gene. pMB017 is a derivative of pMB001 created by filling in the *Bam*H I site distal to the *MIF2* open reading frame with Klenow. pMB027 was constructed as described for pMB024 except that the target vector was pMB025 instead of pMB017. pMB025 was constructed as described for pMB017 except that the base vector was S26. pMB030 was constructed by inserting the complete *MIF2* gene on a 2.6-kb *Pst* I fragment into the CEN4 ARS1 *URA3* vector pEMBLYC32-12, which was constructed by C. Mann and is a member of the pEMBLY plasmid family (Baldari and Cesareni, 1985). pMB031 was constructed similarly to pMB030 but contains the 2.6-kb *Pst* I fragment in the opposite orientation. pMB034 was constructed from pMB031 by deleting a 0.7-kb *Sph* I-*Pst* I fragment of the *MIF2* insert, leaving behind in the vector a 1.9-kb *Pst* I-*Sph* I fragment containing the *MIF2* gene. pMB038 was constructed by inserting the *MIF2* gene contained on a 1.9-kb *Sph* I fragment into the *Sph* I site of pTC3, a CEN3 ARS1 *TRP1* vector constructed by K. Nasmyth by insertion of a 2.0-kb *Hind* III-*Bam*H I CEN3 fragment into the *Pvu* II site of YRp7. The 1.9-kb *Sph* I fragment consists of the *MIF2* gene on a 1.9-kb *Pst* I-*Sph* I fragment plus the region of the pMB030 polylinker sequence between the vector *Pst* I and *Sph* I sites.

Table I. Yeast Strains

Strain		Genotype
LH330SD*	α	*ade2 leu2 trp1 hom3 ura3 can1 fcy1 sap3 (lys5 + cyh2 + ade +)/(+ aro2 + + ade3)*
mif2-3B	a	*mif2-3 his3 ade2 trp1 leu2 ura3 can1 sap3*
4050-15	a	*leu2 trp1*
4050-15-γ1	a	*leu2 trp1 MIF2::TRP1*
4053-3-4Z1	α	*his7 ura3 MIF2::URA3*
4076-27	a	*his7 ura1*
5371-8-3	α	*ura3*
5371-10-2	a	*ura3*
6716-7-1	a	*his3 ade2 trp1 leu2 ura3 can1 sap3*
6730	a/α	*his3/his3 ura3/ura3 +/mif2::HIS3 +/leu2 +/met2 +/sap3*
6764-181	α	*his3 ura3 trp1 leu2 met2 can1 sap3 mif2::HIS3, plasmid pMB030*
6767-C1-A*	α	*mif2-2 ade2 leu2 trp1 hom3 ura3 can1 fcy1 sap3 (lys5 + cyh2 + ade6 +)/(+ aro2 + + ade3)*
6768-D4-A*	α	*mif2-3 ade2 leu2 trp1 hom3 ura3 can1 fcy1 sap3 (lys5 + cyh2 + ade6 +)/(+ aro2 + + ade3)*
6783-D-4	a	*ura3 leu2 his3 his7 can1 sap3 MIF2::URA3*
6796-5-2	a	*mif2-3 trp1 leu2 ura3*
6799	a/α	*mif2-3/mif2-3 can1/+ hom3/+ ura3/ura3 trp1/+ his3/+ his7/+ sap3/sap3*
6801	a/α	*MIF2/MIF2 can1/+ hom3/+ ura3/ura3 leu2/leu2 his3/+ his7/+ sap3/sap3*
6815	a/α	*mif2-5/mif2-5 can1/+ hom3/+ ura3/+ trp1/+ his3/+ his7/+ sap3/sap3*
6810-2-3	a	*mif2-6 his3 trp1 leu2 ura3 can1 sap3*
6818-1-1	α	*mif2-2 ura3 leu2 sap3*
6832	a/α	*cdc17/cdc17 can1/+ hom3/+ ura3/+ leu2/+ his7/his7 sap3/+ ura1/+*
6836	a/α	*mif2-2/mif2-2 can1/+ hom3/+ ura3/+ leu2/+ trp1/+ his3/+ ade2/+*
6848-9-4	α	*mif2-2 ura3*
6849-8-4	α	*mif2-3 ura3 sap3*
6849-10-1	a	*mif2-3 ura3*
6858-19-2	α	*mif2-5 ura3*
6881-13-1	α	*cdc16 ura3*
6886B-14-3	α	*mif2-6 ura3*
6898-3-2	α	*cdc9 ura3*
6918-8-2*	α	*mif2-3 his7*

* Not of congenic A364a strain background.

Non-complementation of a mif2 Null Mutation by MIF2 DNA Sequences

The *MIF2* 4.4-kb *Bam*H I fragment from the multicopy chromosome destabilizing plasmid S26 (Meeks-Wagner et al., 1986) was cloned into two different centromere-*URA3* plasmids to form pMB001 and pMB002, which

were transformed into 6730, a *ura3/ura3* diploid heterozygous for a lethal disruption of *MIF2* formed by insertion of the *HIS3* gene (Meeks-Wagner et al., 1986). Transformants were sporulated and their progeny scored for viable spores per tetrad. Viability segregated 2:2 for both pMB001 and pMB002, the same result obtained for control transformants containing either of the pMB001 and pMB002 parent centromere-*URA3* vectors JK007 and YCp50, which lack the *MIF2* insert. The surviving spores were either His^-Ura^- or His^-Ura^+, indicating that none contained the *HIS3* disruption of *MIF2* and that the centromere plasmid segregated independently of the disruption. Because centromere plasmids segregate 2:2 in meiosis (Clarke and Carbon, 1980), a mixture of tetrads segregating viability 4:0, 3:1, and 2:2 was expected if either pMB001 or pMB002 were able to complement the *MIF2* disruption; furthermore, some of the viable spores would have been His^+Ura^+. Since neither of these conditions was fulfilled, the 4.4-kb *Bam*H I fragment must not encode a complementing *MIF2* gene.

Cloning of MIF2

To obtain a complete *MIF2* gene, DNA flanking the 4.4-kb partial gene was cloned by integrative transformation. Plasmid S26, which contains the 4.4-kb partial *MIF2* gene and the bacterial β-lactamase gene, was integrated at the *MIF2* locus, forming duplicated copies of *MIF2* flanking bacterial DNA, as verified by Southern analysis. Genomic DNA was isolated, restricted with *Eco*R I, ligated, and ampicillin resistant transformants were selected in *E. coli*. (*Eco*R I was chosen because it cuts within plasmid sequences outside of the β-lactamase gene but does not cut within the partial *MIF2* gene fragment as diagrammed in Fig. 1. Genomic mapping had indicated that the nearest *Eco*R I site flanking the partial gene was ~3 kb away.) Plasmids isolated from the ampicillin resistant transformants contained 3.05 kb of novel DNA flanking the original 4.4-kb *MIF2* fragment.

Northern Analysis

Total RNA was isolated from exponentially growing yeast cells (Sclafani and Fangman, 1984). Poly A^+ RNA was isolated from total RNA using poly U sepharose. RNA samples were denatured with glyoxal, separated by electrophoresis through a 1% agarose gel in 10 mM sodium phosphate buffer (pH 7.0), transferred to a nylon membrane (Nytran, Schleicher & Schuell, Inc., Keene, NH) by Northern blotting, and hybridized to the *MIF2* 2.6-kb *Pst* I fragment.

DNA Sequencing

The sequence of both strands of the *MIF2* gene was determined by the dideoxy chain termination method (Sanger et al., 1977) using double-stranded plasmids and the Sequenase DNA Sequencing Kit (Un. States Biochemical, Cleveland, OH). A nested set of deletions was prepared by Exonuclease III digestion (Henikoff, 1984), and commercially available primers were used to initiate polymerization. Where gaps existed, 17-mer oligonucleotides based on previously generated *MIF2* sequence were synthesized and used as primers. Homology searches of sequence databases were performed using the Intelligenetics FASTDB program (Brutlag et al., 1990).

Isolation of Conditional Mutants

pMB038 was mutagenized in vitro with hydroxylamine (NH_2OH; Sigma Chem. Co.) essentially as described (Rose and Fink, 1987). 3.3 μg of DNA in 2 μl of TE, pH 8.0, was added to 100 μl of hydroxlamine solution, which consists of 0.09 g NaOH and 0.35 g NH_2OH-HCl in 5 ml ice cold H_2O, made immediately before each mutagenesis. The DNA was incubated for 30–120 min at 75°C (Belfort and Pedersen-Lane, 1984), depending on the desired frequency of mutagenesis. Because pMB038 contains two markers that can be selected in *E. coli* strain JA194, the β-lactamase gene which confers resistance to ampicillin and the yeast *TRP1* gene which complements the *E. coli trpC* mutation, the degree of mutagenesis can be assessed in bacteria. Amp^R transformants were screened for loss of *TRP1* function by replica plating to medium lacking tryptophan (M9 + 64 mg/liter leucine). When DNA was mutagenized for 60 min, for example, the frequency of Trp^- mutants was 2%.

Mutagenized pMB038 was transformed into 6764-181, a haploid yeast strain containing both a lethal genomic disruption of *MIF2* and pMB030, a CEN4 *URA3* plasmid containing *MIF2* sequences that complement the lethal defect of the disruption allele. Transformants were selected on C − uracil − tryptophan medium at 23°C, and then patched to C medium to allow loss of the *URA3* plasmid. After several days growth at 23°C, the plasmids were shuffled (Mann et al., 1987) by replica plating to C − tryptophan plates containing 5-fluoroorotic acid (SCM Chemicals, Gainesville, FL; Boeke et al., 1984), which selects against cells with *URA3* function, at 14, 23, and 36°C. Only cells lacking pMB030 and harboring mutagenized pMB038 will grow on this medium. Of 4,110 transformants screened, 44 were capable of growth at 23°C but not 36°C, and 7 could grow at 23°C but not 14°C. By testing for conditional growth on C plates, 13 heat sensitive strains were found to have defects in the *TRP1* gene whereas none of the cold sensitive strains were defective in *TRP1* function. Linkage of the conditional defect to pMB030 in the remaining 31 heat sensitive and 7 cold sensitive candidates was determined by isolating plasmid from the temperature sensitive yeast strains, transforming *E. coli* with the rescued plasmids, isolating plasmid DNA, retransforming 6764-181, and testing for conditional growth. After this screen, 17 plasmid-linked heat sensitive and 3 cold sensitive mutants remained.

Transfer of Plasmid-linked Mutations into the Genome

Plasmid-linked *mif2* mutations were transferred into the yeast genome by using a two step plasmid integration/excision gene replacement strategy (Scherer and Davis, 1979). 1.9-kb *Sph* I fragments containing the mutagenized *MIF2* gene (consisting of a 1.9-kb *Sph* I–*Pst* I *MIF2* fragment plus polylinker sequence from pMB038 to provide the second *Sph* I site) were isolated from six different temperature sensitive mutant pMB038 plasmids and cloned into the *Sph* I site of the yeast *URA3* integrating vector YIp5 (Struhl et al., 1979). The resulting plasmids were cut with *Bam*H I to target integration to the *MIF2* locus and transformed into either 6716-7-1 or LH330SD. Integrants were selected on C − uracil medium at 23°C. Plasmid excisions were selected on C + 5-fluoroorotic acid medium at 23°C. To identify temperature sensitive isolates, excision events were screened for the ability to grow on C medium at 36°C. For one of the six mutant plasmids, temperature sensitive excisions could not be obtained. Genomic DNA was isolated from four of the five temperature sensitive excision strains as well as the duplication strains from which they were derived, digested with *Bam*H I, and subjected to Southern analysis using a 2.6-kb *Pst* I *MIF2* fragment as probe. The predicted number and sizes of bands appeared for the alleles designated *mif2-2*, *mif2-3*, *mif2-5*, and *mif2-6* as well as their progenitor duplication strains, verifying that the gross structure of DNA at the integration/excision site was as expected, and that these events had occurred at the *MIF2* locus and not at an unlinked site.

Linkage of the five putative *mif2* temperature sensitive mutations 60-23-4, *mif2-2*, *mif2-3*, *mif2-5*, and *mif2-6* to the *MIF2* locus was assessed by crossing mutants to one of the *MIF2* strains 4053-3-4Z1, 4050-15-γ1, or 6783-D-4, all of which contain either *URA3* or *TRP1* integrated adjacent to *MIF2*. Heterozygous diploids were then sporulated and random spores were selected by plating to appropriate medium. All five strains showed complete cosegregation of temperature sensitivity with uracil or tryptophan auxotrophy and so were classified as linked to the *MIF2* locus. Verification that an allele belonged to the *mif2* complementation group was obtained by complementation testing to another temperature sensitive *mif2* allele and requiring that the heteroallelic diploids be temperature sensitive. Only 60-23-4 failed this test and was therefore not classified as an allele of *MIF2*. 2:2 segregation of the temperature sensitive defect was demonstrated by tetrad analysis of each *mif2* allele when crossed to an *MIF2* strain.

Flow Cytometry

Yeast cells were prepared for flow cytometry as described by Hutter and Eipel (1979). 5371-8-3 and 6848-9-4 were grown in C medium to a density of ~4 × 10^6 cells/ml, and then either fixed immediately or shifted to the restrictive temperature for 3 h and 20 min and then fixed. Cells were fixed in 70% ethanol at room temperature for 1 h, washed in PBS, incubated in PBS containing 1 mg/ml RNase A for 1 h at 37°C, washed in PBS, and stained overnight at 4°C with 50 μg/ml propidium iodide (Sigma Chem. Co.). Immediately before flow cytometry, cells were washed in PBS containing 5 μg/ml propidium iodide.

Microcolony Assay

The microcolony assay was used to assess the viability of strains as described for each experiment. In general, strains were grown to log phase in C medium, treated in a specific way, diluted in minimal medium, sonicated briefly, and then plated to C or other medium at a specified temperature. Viability was determined by scoring 200–400 individual cells on each plate by microscopic examination after 1–2 d growth and calculating the

fraction of cells unable to form a colony, which is readily apparent after this length of time. Cells not capable of successfully growing to a colony generally arrest as microcolonies of 1–30 cells, depending on the specific strain and experimental treatment.

Correlation of Lethality with Bud Morphology

6796-5-2 was grown to a density of 5×10^6 cells/ml in C medium at 23°C, and then shifted to 37°C for 3 h. Cells were sonicated and plated to very thin C agar plates at 23°C. Using a microscope, the position of cells and whether they were unbudded, small budded, or large budded was scored and the same cells rescored for whether they had formed a colony 24 and 48 h later.

Chromosome Segregation Assays

MIF2-overproducing plasmid transformants of LH330SD, a haploid strain disomic for chromosome VII, were assayed for the frequency of chromosome VII loss as previously described (Meeks-Wagner et al., 1986). The rate of VII loss in LH330SD and the LH330SD-derived *mif2* strains 6767-C1-A and 6768-D4-A was calculated by the method of the median (Lea and Coulson, 1949) using data gathered in the following way. Each strain was streaked for single colonies on a YEPD plate and incubated at 23, 30, 32, or 34°C overnight. Fifteen colonies were picked from each plate by covering the entire colony with the end of a pasteur pipette and pressing downward such that the colony and agar underlying it become contained on an agar plug within the pipette. Agar plugs were transferred into 1 ml of −N medium, vortexed, and sonicated to suspend and separate cells. To determine the average colony size, aliquots of each sample were pooled and plated to YEPD at 23°C. Another aliquot of each sample was plated at 23°C on YEPD medium + cycloheximide, which selects for both chromosome VII loss and recombination events, distinguishable by their white or red color. A third aliquot was streaked to YEPD at 23°C to determine the color of each original colony. Colonies testing white were excluded from calculations because they were derived from cells that had already lost one copy of chromosome VII. The rate of loss of chromosome V in dipoid strains was also determined by the method of the median. Chromosome V loss events in (*can1 hom3*)/(+ +) diploids were selected on C − arginine + canavanine medium and distinguished from recombination events by their inability to grow on C − methionine medium due to uncovering of the *hom3* marker, as previously described (Hartwell and Smith, 1985; Meeks-Wagner and Hartwell, 1986).

MBC Supersensitivity Assays

Liquid cultures were grown to saturation in YM-1 medium and 2.5 μl of each spotted and streaked in a defined sector (one sixth of a 9-cm petri plate) on prewarmed YEPD plates containing either 0, 10, 15, or 20 μg/ml MBC. After 3–4 d incubation at either 23, 28, 30, 32, 34, or 36°C, *mif2* strains were scored for the degree of growth compared to a congenic *MIF2* strain. Strains tested included 6716-7-1, 5371-10-2, 4076-27, 6818-1-1, *mif2-3*B, 6810-2-3, and 6918-8-2. Quantitative data were obtained by growing strains to a density of 2×10^6 cells/ml in C medium, sonicating briefly, and plating to C medium containing 20 μg/ml MBC, which had been added to the liquid agar medium from a 10 mg/ml stock solution in DMSO immediately before pouring. Viability of cells was assessed by the microcolony assay. DMSO alone at this concentration had no significant effect on cell viability.

Fluorescence Microscopy

Strains were grown in C medium to a concentration of $\sim 2 \times 10^6$ cells/ml at 23°C before either fixing or shifting to the restrictive temperature. Preparation of cells for indirect immunofluorescence was essentially as described (Baum et al., 1988) with several modifications. For each sample, 6 μl of 0.25 μg/ml polylysine was dried onto an area of ~5 mm^2 on the surface of a glass microscope slide before addition of fixed cells. The rat anti-yeast α-tubulin monoclonal antibody YOL1/34 (Accurate, Westbury, NY; Kilmartin et al., 1982) was diluted 1/650 and 10 μl added to cells after attachment to the slide. After a 12-h incubation at room temperature, slides were washed, 10 μl of a 1:100 dilution of FITC-conjugated goat anti-rat IgG antibody (Accurate) containing 1 μg/ml 4′,6-diamidino-2-phenylindole (DAPI; Sigma Chem. Co.) was added, and cells were incubated for 5–7 h at room temperature. Cells were counterstained with Evans Blue (Sigma Chem. Co.) for 5 min to allow visualization of cell outlines. Cells were viewed on a Nikon Microphot microscope equipped for epifluorescence. Mother cells were distinguished from daughter buds in large budded 6849-8-4 cells by a 2 1/2-h incubation in 0.001% calcofluor (Cyanamid, Bound Brook, NJ) at room temperature after formaldehyde fixation.

Electron Microscopy

6849-10-1 was grown to a density of 2.5×10^6 cells/ml in C medium at 23°C, and then shifted to 37°C for 3 1/3 h. Fixation, embedment, and electron microscopy were performed according to previously described methods (Byers and Goetsch, 1991). Several efforts were made to improve contrast between the spindle fibers and cytoplasm, and the best data are presented. The low contrast appears to be caused by characteristics of the *mif2* A364a strain.

Results

Cloning of MIF2

The 4.4-kb *Bam*H I fragment that was originally cloned by Meeks-Wagner et al. (1986) and shown to destabilize chromosomes when overexpressed was tested for its ability to complement a lethal insertion mutation at the *MIF2* locus and found to be incapable of doing so (see Materials and Methods). Reasoning that the 4.4-kb fragment might contain only a portion of the *MIF2* gene, we cloned additional DNA from the *MIF2* region by integrative transformation (Fig. 1 and Materials and Methods). A 7.4-kb fragment consisting of the 4.4-kb *MIF2* fragment and an adjacent 3.0 kb *Bam*H I fragment of newly isolated DNA was cloned into both a centromere-*URA3* plasmid and the multicopy ARS plasmid YRp7, forming pMB024 and pMB027.

pMB024 was transformed into 6730, a diploid heterozygous for a lethal *HIS3* disruption of the *MIF2* gene. After sporulation of transformants, viability was found to segregate 4:0 (6 tetrads), 3:1 (15 tetrads), and 2:2 (24 tetrads), as would be expected for a centromere plasmid containing a functional copy of the *MIF2* gene. In all cases where a 4:0 pattern was observed, two of the viable spores were His^-Ura^-, indicating they carried the undisrupted *MIF2* gene but no plasmid, and two of the spores were His^+Ura^+, indicating they contained the *mif2::HIS3* disruption allele and a complementing centromere-*URA3* plasmid. Whether *MIF2* is essential for mitotic growth and not simply spore germination was tested by assaying plasmid stability in His^+Ura^+ and His^-Ura^+ spores. His^- spores contain the wild-type *MIF2* gene and should be able to survive after loss of the centromere-*URA3* plasmid. His^+ spores contain the lethal *MIF2* disruption and therefore should die when they lose the plasmid if *MIF2* is required for vegetative growth. When His^- strains were grown for seven generations without selecting for maintenance of the *URA3* plasmid, ~60% of the viable cells were Ura^+ and therefore contained the plasmid. For His^+ strains, plasmid stability was 100%. Therefore, His^+ cells were not able to lose the plasmid and survive, indicating that *MIF2* is required for mitotic growth. Subcloning experiments further limited the DNA required for complementation to a 1.9-kb *Pst* I–*Sph* I fragment, composed of a 0.55-kb *Sph* I–*Bam*H I fragment contained within the newly cloned DNA and the adjoining 1.35-kb *Bam*H I–*Pst* I fragment from the original 4.4-kb *MIF2* partial gene (Fig. 2).

Map Position of MIF2

MIF2 was localized to chromosome XI by probing CHEF

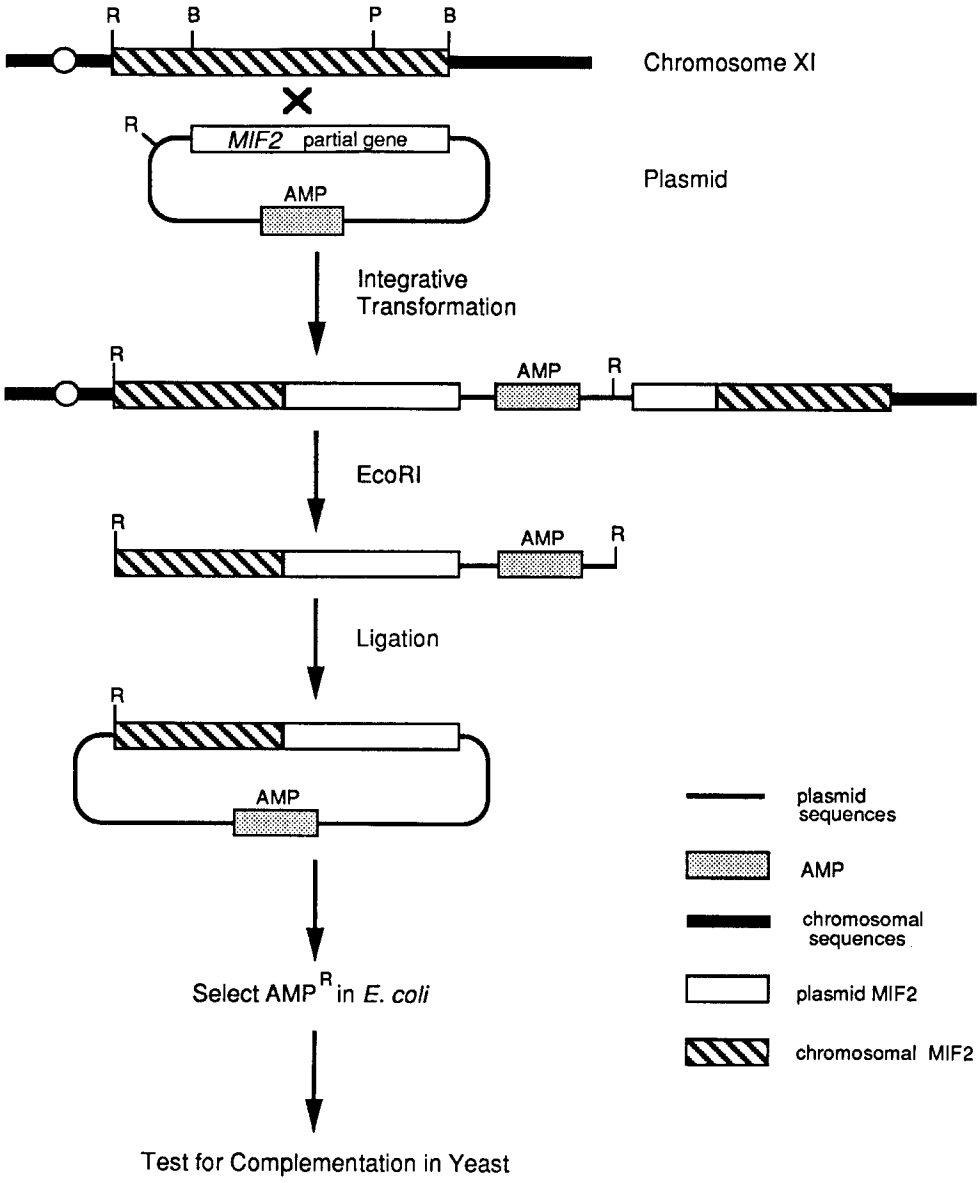

Figure 1. *MIF2* cloning strategy. Plasmid S26, which contains the 4.4-kb *Bam*H I *MIF2* partial gene, the *TRP1* gene from yeast, and the gene conferring ampicillin resistance from *E. coli*, was integrated into the yeast genome by targeted transformation of 4050-15 at the *MIF2* locus, forming duplicated copies of the partial *MIF2* gene. Yeast genomic DNA was isolated from a Trp$^+$ transformant, restricted with *Eco*R I, ligated, and ampicillin resistant transformants were selected in *E. coli*. The newly isolated larger piece of DNA from the *MIF2* region was subcloned into a yeast shuttle vector and tested for complementation of a *MIF2* null allele in yeast. Restriction sites: *R*, *Eco*R I; *B*, *Bam*H I.

blots of yeast chromosomes (Chu et al., 1986) with the 4.4-kb *Bam*H I *MIF2* DNA fragment, contradicting the earlier report that *MIF2* mapped to chromosome IX (Meeks-Wagner et al., 1986). If a CHEF blot was probed with the 2.0-kb *Bam*H I fragment from the original *MIF2* plasmid SC231 (Meeks-Wagner et al., 1986), then only chromosome IX showed hybridization. The original *MIF2* plasmid, therefore, contained two *Bam*H I fragments from different chromosomes. This conclusion was supported by the cloning of novel DNA flanking the 4.4-kb *Bam*H I fragment and demonstration of its non-identity with the 2.0-kb *Bam*H I fragment by restriction analysis and hybridization. The earlier mapping study, therefore, located the genomic position of the 2.0-kb fragment, not the *MIF2* gene.

MIF2 was genetically mapped in relation to several chromosome XI markers (Table II). The resulting data as well as additional distances calculated between non-*MIF2* chromosome XI markers allowed us to map *MIF2* to the left arm of chromosome XI and infer the order of genes as *TRP3-URA1-SUP75-MIF2-CDC16*-(CENXI)-*MET14*. No known essential genes map to this position, indicating that *MIF2* is a previously unidentified gene. The strong data linking *MIF2* to *CDC16* and *SUP75* indicate that *CLY7* should also have shown linkage to *MIF2*. The map position of *CLY7* (Mortimer and Schild, 1985) therefore is placed in doubt.

Overexpression of MIF2

To test the effects of overexpressing the complete *MIF2* gene on chromosome segregation, a multiple copy ARS plasmid containing the intact *MIF2* gene, pMB027, was transformed into LH330SD, a chromosome VII disome genetically marked for assaying loss of VII (Meeks-Wagner and Hartwell, 1986). pMB027 increased chromosome VII loss to 12-fold higher levels than did the vector plasmid YRp7. S26, a YRp7-derived plasmid containing the partial *MIF2* gene, increased chromosome VII missegregation 75-fold above vector levels. Strains overexpressing the partial gene also showed an increased proportion of cells in the G_2 and M phases of the cell cycle (44%) compared to the proportion seen in strains containing the vector plasmid (26%), as de-

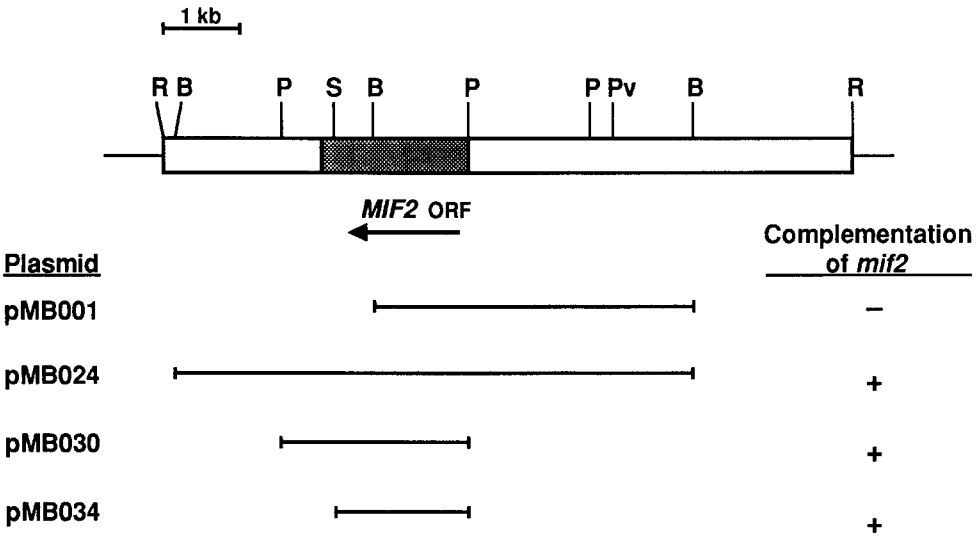

Figure 2. Restriction map of the *MIF2* region and plasmid complementation analysis of a *mif2* null allele. The shaded region indicates the DNA sequenced. The arrow beneath the map specifies the *MIF2* coding region. The bars indicate the DNA fragments from the *MIF2* region that were tested for complementation. Plasmids were transformed into 6730, a diploid heterozygous for a null allele of *MIF2*. Transformants were sporulated and scored for complementation. Plus (+) and minus (−) signs indicate the ability of the indicated plasmids to complement the *mif2* null allele. *R*, *Eco*R I; *B*, *Bam*H I; *P*, *Pst* I; *S*, *Sph* I; *Pv*, *Pvu* II; *ORF*, open reading frame.

termined by bud morphology and intracellular location of the nuclear DNA.

Molecular Analysis of MIF2

Northern analysis of yeast poly A^+ RNA identified two transcripts of 2.05 and 1.8 kb that hybridized to a 2.6-kb *Pst* I DNA probe corresponding to the functional region of *MIF2*. No bands were visible when total RNA was hybridized to a *MIF2* probe, indicating that these RNAs are relatively scarce and explaining why no *MIF2* transcripts were identified in previous attempts (Meeks-Wagner et al., 1986).

A 2,161-bp region of DNA containing the sequences that confer *MIF2* complementing activity was sequenced and found to contain a single long open reading frame (Fig. 3). The predicted length of the protein is 549 amino acids counting from the first of four in-frame methionines within the initial 55 amino acids. Of the four potential start codons, which are located at positions 1, 4, 28, and 45, the first two are situated within a poor context for efficient translation initiation (ACTCATGG and TTATATGA), whereas the second two are located within a context associated with highly efficient translation initiation (CAGCATGG and CAGTATGA), (Kozak, 1984). The predicted molecular weight of the protein beginning at the first in-frame methionine is ~62.5 kD. The partial *MIF2* gene that causes high levels of chromosome loss when overexpressed contains the NH_2-terminal 364 amino acids of the deduced protein sequence.

An unusual feature of the putative *MIF2* gene product is its high number of acidic residues. Whereas acidic amino acids comprise 11.2% of the average eukaryotic protein (Doolittle, 1986), the Mif2 protein contains 20.6% glutamic and aspartic acid residues. The predicted pI of the Mif2 protein is 4.5. Particularly striking is a highly acidic region extending from position 178–263 composed of 42% acidic residues and only one basic amino acid. No significant codon bias was detected. The Codon Adaptation Index (CAI) value for the Mif2 protein is a fairly low 0.142 (Sharp and Li, 1987). Because low CAI values correspond to low levels of gene expression, the *MIF2* gene is likely to be expressed at low levels.

The deduced Mif2 protein sequence was compared to the protein sequences contained in the Swiss-Prot (release 21) and PIR (release 31) databases as well as to translated sequences from the GenBank nucleic acid database (release 71), but no extensive homologies were found. A 12-amino acid perfect match beginning at amino acid 352 was found between Mif2 and the *Drosophila* D1 chromosomal protein, which binds double-stranded AT rich DNA (Levinger and Varshavsky, 1982). Within the matching sequence is a motif required for AT DNA binding by the HMGI family of mammalian chromosomal proteins (Lund et al., 1987; Reeves and Nissen, 1990). Synthetic peptides containing this motif have been shown to specifically bind AT DNA in vitro (Reeves and Nissen, 1990). D1 contains eleven of the AT DNA-binding motifs (Ashley et al., 1989), HMGI contains three motifs, and Mif2 contains one. The D1, human HMGI,

Table II. Map Position of MIF2

Interval	PD	NPD	TT	Distance (cM)
MIF2-TRP3	107	45	329	62.3
MIF2-URA1	28	10	75	59.7
MIF2-MET14	37	12	101	57.7
MIF2-SUP75	80	3	66	28.2
MIF2-CDC16	55	1	55	27.5
MIF2-MET1	16	11	50	75.3
MIF2-CLY7	14	11	41	81.1
MIF2-MAK9	8	4	47	60.2
TRP3-URA1	101	0	10	4.5
SUP75-TRP3	40	10	96	53.4
MAK9-TRP3	26	2	31	36.4
CLY7-TRP3	9	8	51	72.8

Linkage of *MIF2* to chromosome XI markers was assessed by crossing either a strain in which the *URA3* gene had been integrated immediately adjacent to the *MIF2* locus or a temperature sensitive *mif2-3* mutant to strains bearing the indicated genes. The resulting diploids were sporulated and their tetrads dissected. Map distance was calculated according to Perkins et al., 1949. *PD*, Parental Ditype; *NPD*, Non-parental Ditype; *TT*, Tetratype; *cM*, centiMorgans.

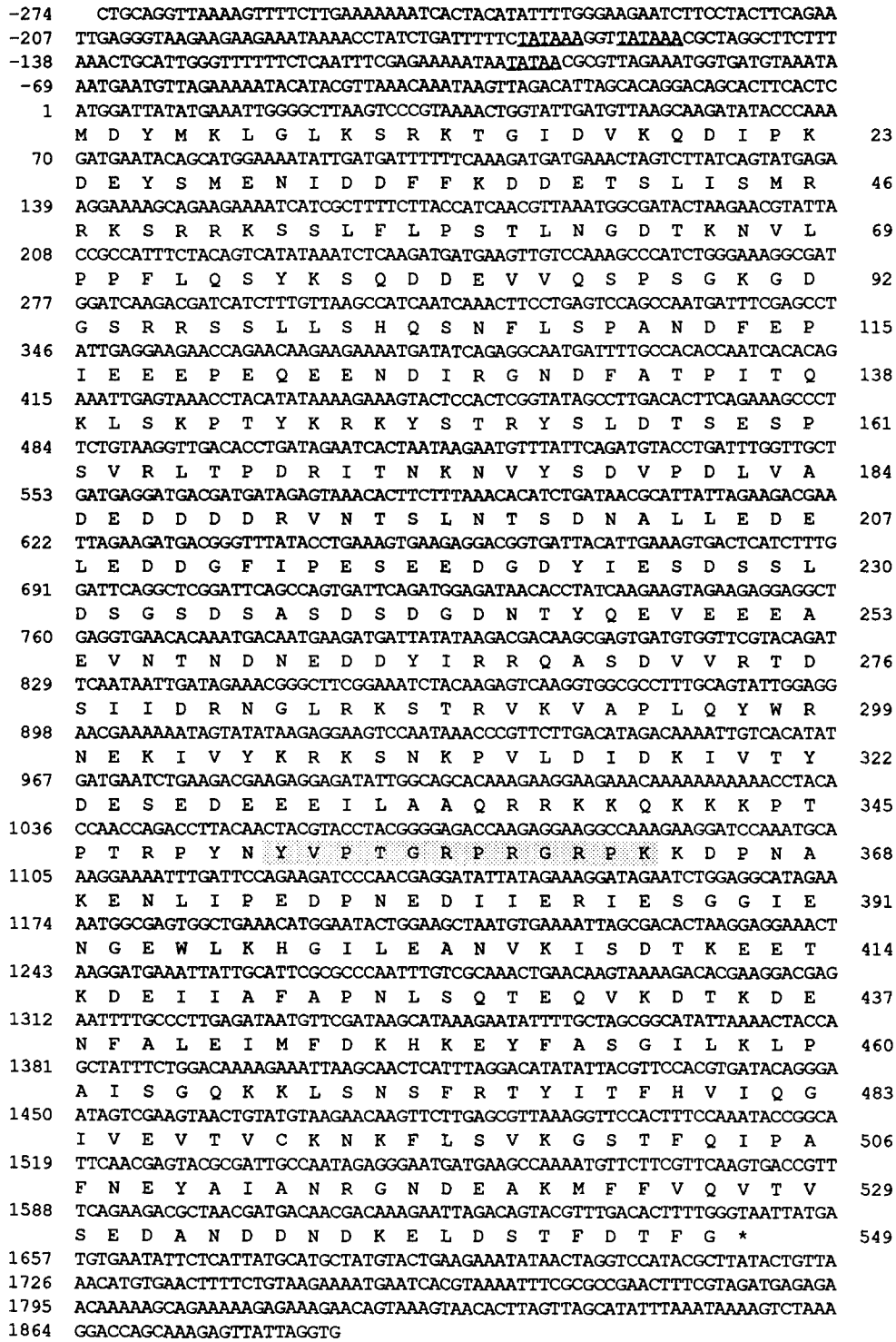

Figure 3. DNA sequence of the *MIF2* gene. The sequence of 2161 bases of DNA containing the *MIF2* open reading frame is shown along with the predicted amino acid sequence of the gene product. Numbers in the left margin refer to the DNA sequence, with 1 designated as the first base of the first in-frame methionine codon. Numbers in the right margin indicate the amino acid sequence. The TAA stop codon is indicated by an asterisk (*). Potential TATA boxes at −167, −158, and −99 are underlined. The *Pst* I, *Bam*H I, and *Sph* I sites are located on positions −274, 1093, and 1675, respectively. The 12-amino acid sequence with perfect homology to *Drosophila* D1 protein is contained within the shaded box. These sequence data are available from EMBL/GenBank/DDJB under accession number Z18294.

mouse HMGY, and Mif2 DNA-binding motifs are compared in Fig. 4.

The Mif2 protein also contains four sequences fitting the most preferred consensus site for phosphorylation by cAMP dependent kinase, R-R/K-X-S/T (Kennelly and Krebs, 1991), which are located at amino acid positions 46 (R-R-K-S), 50 (R-R-K-S), 95 (R-R-S-S), and 285 (R-K-S-T). The sequence T-P-T-R at amino acid 345 is potentially a $p34^{cdc2}$ kinase (gene product of *CDC28* in *S. cerevisiae*) phosphorylation site (Moreno and Nurse, 1990).

Isolation of Temperature Sensitive mif2 Alleles

The question of what happens when cells have a deficit rather than a surplus of *MIF2* function was examined by isolating conditional lethal alleles of *MIF2*. The centromere plasmid pMB038, which contains *MIF2* sequences capable of complementing a lethal disruption allele, was mutagenized in vitro, and 17 heat sensitive and 3 cold sensitive plasmid-linked mutants were recovered using a plasmid shuffle scheme (see Materials and Methods). Six of the mutant

MIF2, 357-364	R P R G R P K K
HMGI (human), 28-35	R G R G R P R K
HMGI (human), 56-63	R P R G R P K G
HMGI (human), 82-89	K P R G R P K K
HMGY (mouse), 28-35	R G R G R P R K
HMGY (mouse), 45-52	R P R G R P K G
HMGY (mouse), 71-78	K P R G R P K K
D1, I	K K R G R P S K
D1, II	K K R G R P A K
D1, III	G Q R G R P P K
D1, IV	K G R G R P K S
D1, V	R K A G R P K K
D1, VI	R P V G R P S A
D1, VII	R G L G R P K K
D1, VIII	K K R G R P P Q
D1, IX	R P R G R P K A
D1, X	K K R G R P S L
D1, XI	K P R S R P A K
consensus:	R/K X R G R P K K

Figure 4. Comparison of AT DNA-binding motifs from Mif2, Human HMGI, Mouse HMGY, and *Drosophila* Dl proteins. The Mif2 motif shares 100% homology with a Dl 12–amino acid sequence containing the DNA-binding motif in repeat IX (Ashley et al., 1989). HMGY is an alternatively spliced mouse homolog of HMGI (Johnson et al., 1988, 1989). Shaded residues indicate matches with a consensus motif.

genes were introduced into yeast as genomic replacements of the resident wild-type *MIF2* gene in a standard two step plasmid integration/excision procedure. Putative *mif2* mutants were tested for linkage to the *MIF2* locus, noncomplementation of other *mif2* temperature sensitive alleles, and 2:2 segregation for temperature sensitivity. The four alleles that fulfilled these requirements, *mif2-2*, *mif2-3*, *mif2-5*, and *mif2-6*, are all recessive and represent four distinct alleles both because of their independent isolation and the differing temperatures required to arrest their growth.

Arrest of Cell Division by mif2 Mutants

mif2 mutants were grown to exponential phase at 23°C, shifted to their restrictive temperature for three hours, and scored for bud morphology by light microscopy. *mif2-3* cells arrested cell division with ~18% unbudded, 7% small budded, and 75% large budded cells. (A large budded cell is defined as having a bud at least 3/4 the size of the mother cell.) The other *mif2* alleles also arrested predominantly as large budded cells, *mif2-2* with 76%, *mif2-5* with 60%, and *mif2-6* with 74%. In contrast, only 28% of wild-type cells grown at 37°C had large buds. The large budded morphology is typical of cells arrested in the S, G_2, or M phases of the cell cycle. Arrested mutant cells were larger in size than congenic *MIF2* cells grown under similar conditions, a characteristic of cell division cycle (*cdc*) strains that are blocked in cell division but continue protein synthesis (Hartwell, 1967; Johnston et al., 1977). *mif2* cells did not arrest growth with as uniform a terminal morphology as classical cell cycle mutants such as *cdc9* and *cdc16*, which halt cell cycle

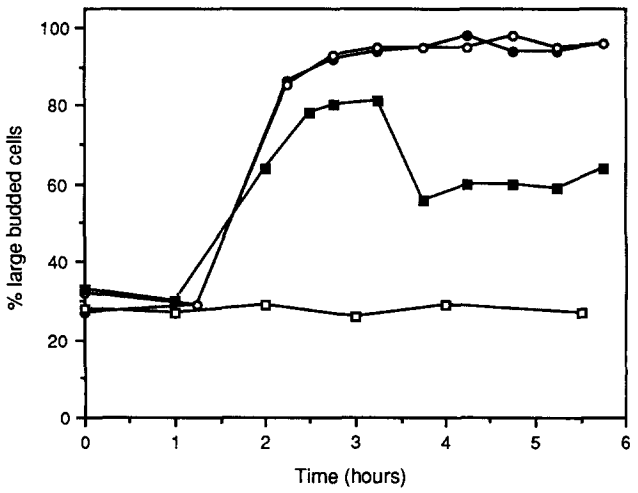

Figure 5. Stability of cell cycle arrest in a temperature sensitive *mif2* mutant. *mif2-3* (■), *cdc9* (●), *cdc16* (○), and wild-type (□) strains were grown to exponential phase in C medium at 23°C and shifted to 37°C. The fraction of the cell population having a large budded morphology was scored by light microscopic examination at timed intervals after the temperature shift. Strains used: 6898-3-2, 6881-13-1, 6849-10-1, 5371-10-2.

progression with >90% large budded cells at the restrictive temperature (Fig. 5). To see if presynchronization of *mif2* cells could increase the uniformity of the arrest morphology, *mif2-3* cells were synchronized as unbudded G_1 cells with the yeast mating pheromone α-factor, and then released from the α-factor block simultaneously with a temperature increase to 37°C. The ensuing profile of arrest morphologies was similar to that given by asynchronously grown *mif2-3* cultures, indicating that the heterogeneity in arrest is not due to multiple execution points. With increasing times at the restrictive temperature, the fraction of large budded cells decreased (for example, to 60% after 5 h for *mif2-3*) and the unbudded and small budded populations increased, indicating that the unbudded and small budded cells originate by cytokinesis of the large budded cells. In contrast, >90% of *cdc9* and *cdc16* cells remained large budded for at least six hours after a shift to the restrictive temperature (Fig. 5). Furthermore, when exponentially growing *mif2-3* cells were plated at 38°C and scored 8 h later, only 6 out of 310 microcolonies consisted of an unbudded cell, suggesting again that the unbudded cell population results from division of large budded cells. The heterogeneity of arrest observed for all four *mif2* alleles may be characterisitic of *MIF2* loss of function or alternatively could reflect leakiness of the alleles isolated.

mif2-induced Cell Lethality

When *mif2* cells were held at the restrictive temperature, they rapidly lost viability (Fig. 6). If *MIF2* function is required only during a specific stage of the cell cycle, then mutant cells not actively progressing through the cell cycle should have no requirement for *MIF2* and remain viable at the restrictive temperature. If, however, *MIF2* function is required continuously during the cell cycle, then loss of viability will not require progression through the cycle. To distinguish between these possibilities, *mif2* cells were prevented

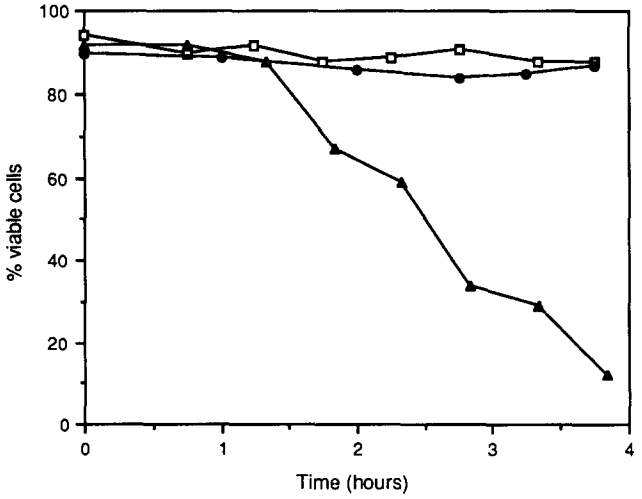

Figure 6. Viability of *mif2* in α-factor. 6849-10-1 was grown to a cell density of ~10^6 cells/ml in C medium, pH 3.5, at 23°C. The culture was divided into two aliquots. One aliquot was shifted to 37°C. To the other aliquot, α-factor was added to a final concentration of 10^{-6} M, and the cells were allowed to continue growing at 23°C. After 2 1/2 h, the cell population of the α-factor containing culture consisted of 80% unbudded cells; this is considered to be the zero timepoint. Half of this culture was allowed to continue growing at 23°C and the other half was shifted to 37°C. Aliquots were removed from each of the cultures at intervals, diluted into -N medium, treated with 20 μg/ml pronase at room temperature for 5 min to destroy α-factor, and plated to C medium at 23°C. Viability was assessed by the microcolony assay. □: α-factor, 23°C; ●: α-factor, 37°C; ▲: no α-factor, 37°C.

from traversing the cell cycle by arrest with α-factor at 23°C, followed by an increase in temperature to 37°C. After almost four hours at the restrictive temperature, α-factor arrested cells showed no drop in viability, whereas only 12% of control cells to which no α-factor had been added were viable (Fig. 6). This result demonstrates that *MIF2* is not required continuously during the cell cycle but rather has a stage specific function that occurs at some time in the cycle other than the G_1 arrest period.

Although *mif2-3* cells arrest primarily as large budded cells at the restrictive temperature, ~25% of cells pass through this block after 3 h, producing unbudded and small budded cells. When returned to the permissive temperature of 23°C, 47% of large budded cells were able to form viable colonies whereas only 7 and 10% of unbudded and small budded cells, respectively, had this capability. This result suggests that completion of some event after the large budded single nucleus stage, where the majority of *mif2* cells arrest (see below), is lethal in the absence of the *MIF2* gene product.

mif2 Mutants Complete DNA Replication

Because DAPI staining indicated that temperature arrested *mif2* cells have a single mass of nuclear DNA located at the bud neck and therefore might be arrested in either S, G_2, or early M phase (see below), we wished to further define the arrest point by determining whether arrested cells have completed DNA replication. We examined the extent of DNA replication by measuring cellular DNA content with a fluorescence-activated cell sorter (FACS). Flow cytometry

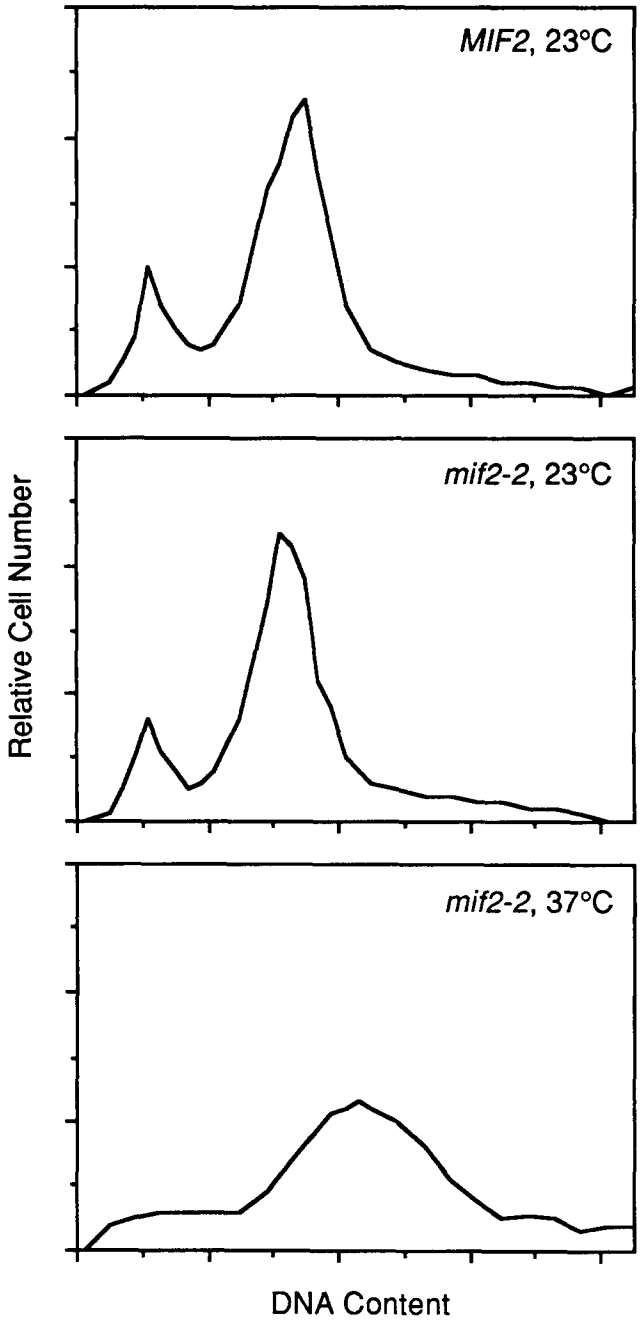

Figure 7. DNA content of *mif2* cells. DNA content was determined by harvesting *MIF2* (5371-8-3) or *mif2-2* (6848-9-4) cells during exponential growth at 23°C and subjecting them to flow cytometric analysis. A portion of the *mif2-2* culture was shifted to 37°C for 3 1/3 h before sampling. Where two peaks appear, the left peak is assumed to represent G_1 cells and the right peak G_2. *MIF2* cells arrested in stationary phase display one peak that aligns approximately with the presumed G_1 peak whereas cells arrested with the microtubule inhibitor MBC have one peak that aligns just to the right of the presumed G_2 peak (data not shown). The rightward displacement of the G_2 peak for both MBC arrested *MIF2* and temperature arrested *mif2-2* cells is probably due to their increased size, because in flow cytometric analysis larger cells may appear to contain more DNA (Cross, 1988; Beach et al., 1988).

Table III. Mitotic Recombination and Chromosome Loss in mif2 Mutants

Genotype*	Chromosome	23°C	30°C	32°C	34°C	36°C
		Rate of mitotic recombination/10^5 cell divisions				
MIF2/MIF2	V	5.46	3.98	ND	3.18	6.24
mif2-2/mif2-2	V	2.43	6.07	ND	6.34	4.49
mif2-3/mif2-3	V	3.04	3.72	ND	4.59	ND
mif2-5/mif2-5	V	1.67	3.51	ND	2.00	ND
cdc17/cdc17	V	1.73	41.3	ND	153	ND
		Rate of chromosome loss/10^5 cell divisions				
MIF2	VII	5.62	3.58	3.07	3.69	ND
mif2-2	VII	95.6	1260	3520	3370	ND
mif2-3	VII	454	1660	5830	ND	ND
MIF2/MIF2	V	5.46	2.38	ND	2.16	1.92
mif2-2/mif2-2	V	11.7	23.4	ND	60.9	32.0
mif2-3/mif2-3	V	43.1	42.7	ND	38.0	ND
mif2-5/mif2-5	V	1.67	12.8	ND	12.2	ND

Rates of mitotic loss of chromosome VII in disomic haploids and of chromosome V in diploids were determined at the indicated temperatures as described in Materials and Methods. The strains used were LH330SD, 6767-C1-A, 6768-D4-A, 6801, 6836, 6799, 6815, and 6832.
* Complete genotypes are given in Table I. *ND*, not done.

of an exponentially growing wild-type strain showed that one population of cells has a G_1 content of DNA and another has a G_2 content. A *mif2-2* strain behaved similarly when grown at 23°C under identical conditions. Temperature arrested *mif2-2* cells displayed a very different profile (Fig. 7). Most cells had a G_2 or greater content of DNA, indicating that the bulk of DNA replication is completed in cells deficient for *MIF2* function. Similar results were obtained with the *mif2-3* mutant. The broad distribution of cells surrounding the G_2 peak may represent aneuploid cells produced by *mif2*-induced mitotic chromosome missegregation (see below). We also tested the X-ray resistance of temperature arrested *mif2* cells, and found it to be typical of cells that have completed the bulk of DNA replication but not chromosome segregation (data not shown), a result that supports the FACS data.

FACS and X-ray analysis do not readily distinguish between cells blocked in G_2 that have completed DNA replication successfully and those whose replicated DNA contains nicks and gaps. Treatments that cause lesions in nuclear DNA such as UV irradiation or limiting cells for gene products involved in DNA metabolism stimulate the recombinogenic repair system of yeast. Elevated levels of mitotic recombination, therefore, can be used as a very sensitive assay to detect deficiencies in DNA replication (Hartwell and Smith, 1985). We measured the levels of mitotic recombination of chromosomes V (Table III) and VII (data not shown) at semipermissive temperatures for several *mif2* alleles, but observed no significant increases above background levels. This result supports the conclusion that *MIF2* is not required for DNA synthesis. In contrast, a *cdc17* strain defective in DNA polymerase I function showed a 10-fold increase in chromosome V mitotic recombination over background levels at 30°C and an 80-fold increase at 34°C, as expected for a mutant unable to complete DNA replication.

Another result suggesting *MIF2* has no role in DNA metabolism is that *mif2 rad9* double mutants arrested cell division as efficiently as *mif2* mutants at the restrictive temperature. The *RAD9* checkpoint gene allows cells to arrest in G_2 to repair potentially lethal DNA damage. *rad9* mutant cells bypass this G_2 arrest (Weinert and Hartwell, 1988). Because most *mif2 rad9* cells do arrest in G_2/M, the *mif2* block is therefore not a *RAD9*-dependent response to DNA damage. Furthermore, *mif2* and *mif2 rad9* cells were equally inviable at the restrictive temperature, demonstrating that *RAD9* plays no role in protecting *mif2* cells from dying as it does for *RAD9*-dependent cell cycle mutants (Hartwell and Weinert, 1989; Weinert and Hartwell, 1993).

MIF2 Is Required for Accurate Chromosome Segregation

The fidelity of chromosome segregation in *mif2* mutants was measured genetically by selecting for chromosome loss events in colonies grown at permissive or semirestrictive temperatures. The rate of chromosome VII loss was determined using a haploid strain disomic for chromosome VII, in which VII missegregations appear as white sectors in a red colony background (Meeks-Wagner and Hartwell, 1986). Even at a permissive temperature of 23°C, *mif2* mutants showed elevated levels of errors in chromosome segregation, exceeding the wild-type rate by 17-fold for *mif2-2* and by 80-fold for *mif2-3* (Table III). This result indicates that *MIF2* function is compromised at the permissive temperature despite the similar growth rates of *mif2* and wild-type strains at this temperature. The rate of chromosome missegregation increased when limitation for *MIF2* gene product became even more severe at higher temperatures. This was indicated qualitatively for chromosome VII by the appearance of increasing numbers of white sectors as the temperature was raised and quantitatively by a rate of loss that exceeds wild-type levels over 1,000-fold at higher temperatures (Table III). The rates of chromosome V missegregation at intermediate temperatures were obtained by measuring the production of chromosome V monosomes in a diploid strain. When compared to wild-type levels, the rate of V loss at 34°C was 28-fold higher in *mif2-2*, 18-fold higher in *mif2-3*, and 6-fold higher in *mif2-5* (Table III). Elevated levels of loss of chromosomes II, III, IV, and XV were also observed but not quantified.

Table IV. Viability on MBC-containing Medium

Temperature	Medium	% viable cells				
		MIF2	*mif2-2*	*mif2-3*	*mif2-5*	*mif2-6*
23°C	C	95	96	97	93	67
	MBC	90	78	95	56	13
28°C	C	93	98	97	98	60
	MBC	99	91	89	64	26
30°C	C	94	99	96	96	50
	MBC	96	87	83	28	12
32°C	C	96	98	88	94	24
	MBC	94	87	60	4	10
34°C	C	94	85	11	40	<0.5
	MBC	97	62	2	1	<0.5
36°C	C	94	29	<0.5	<0.5	<0.5
	MBC	97	2	<0.5	<0.5	<0.5

Cells were grown to a density of 2–3 × 10^6 cells/ml in C medium at 23°C, sonicated briefly, diluted, and plated at the specified temperatures to C medium and C medium containing 20 μg/ml MBC. Viability was assessed by the microcolony assay. The strains used were 5371-8-3, 6848-9-4, 6849-8-4, 6858-19-2, and 6886B-14-3.

mif2 Supersensitivity to the Microtubule Destabilizing Drug MBC

Because microtubule inhibitor drugs of the benzimidazole carbamate family such as MBC act by destabilizing microtubules in yeast (Jacobs et al., 1988), an altered cellular response to such a drug can indicate defects in microtubule function. For example, mutations in the genes encoding β-and α-tubulin can cause benzimidazole carbamate resistance or supersensitivity (Thomas et al., 1985; Huffaker et al., 1988; Schatz et al., 1988). Initially, three *mif2* alleles were tested for sensitivity to MBC by assaying the growth of cells on C medium containing 10, 20, and 40 μg/ml MBC at semipermissive temperatures. Wild-type strains were resistant to 20 μg/ml and sensitive to 40 μg/ml. At semipermissive temperatures, *mif2-2*, *mif2-3*, and *mif2-6* were all supersensitive to MBC for growth when compared to wild-type. *mif2-2* and *mif2-3* were impaired for growth at 20 μg/ml MBC and *mif2-6* at 10 μg/ml MBC. To better assess the MBC supersensitivity of *mif2* strains, a more quantitative test for MBC sensitivity was devised. Exponentially growing strains at 23°C were plated to C and C + 20 μg/ml MBC medium at various temperatures and scored one and two days later for viability using the microcolony assay described in Materials and Methods. A wild-type strain was 90–97% viable at temperatures ranging from 23–36°C on both C medium alone and C + MBC medium. *mif2-2*, *mif2-3*, *mif2-5*, and *mif2-6* displayed varying degrees of supersensitivity (Table IV). For example, at 32°C *mif2-5* was 94% viable on C plates but only 4% viable when grown in the presence of MBC.

MIF2 Is Required for Normal Spindle Structure

mif2 cells were simultaneously stained with anti-tubulin antibodies and DAPI to allow visualization of cellular microtubules and chromosomal DNA by fluorescence microscopy (Fig. 8). The results were tabulated and are presented in Fig. 9. After 3 h at the restrictive temperature, 67% of *mif2-2* and 77% of *mif2-3* cells possessed a single mass of nuclear DNA located at or extending across the neck that connects the mother and large bud (Fig. 8, *D* and *E*, and Fig. 9), indicating that segregation of the chromosomal DNA had not been completed but that nuclear migration had occurred successfully. Only 6–7% of *mif2* cells contained nuclear DNA that

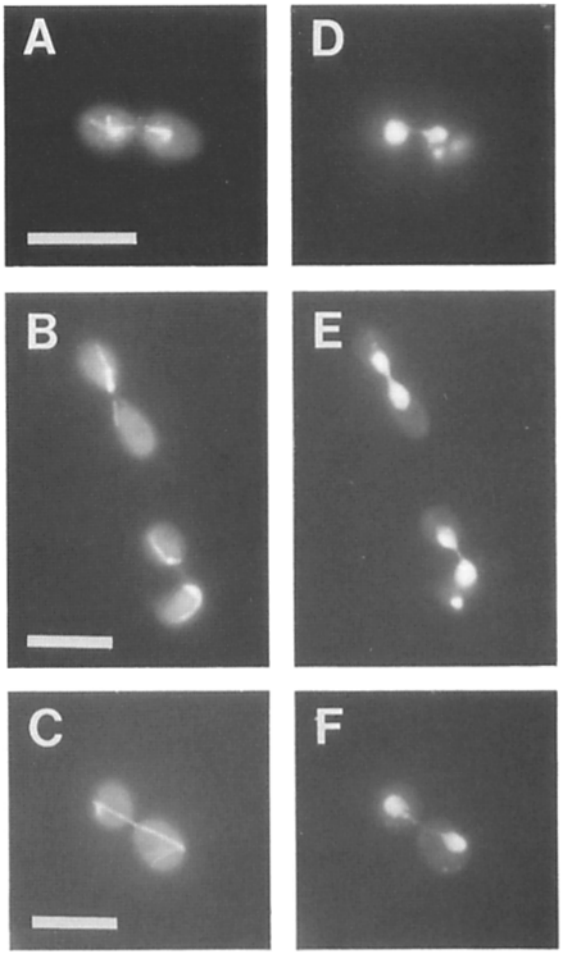

Figure 8. Fluorescence microscopy of *mif2* cells. 6849-8-4 (*mif2-3*) was shifted from exponential growth in C medium at 23°C to 37°C for 3 h, and then fixed and stained with anti-tubulin antibodies (*A*, *C*, and *E*) and DAPI (*B*, *D*, and *F*) as described in Materials and Methods. (*A* and *D*) A larger budded cell with a broken spindle. (*B* and *E*) Two large budded cells, one with an intact, short spindle (*top cell*) and the other with a broken spindle (*bottom cell*). (*C* and *F*) A large budded cell with an elongated spindle. (This morphology appears in less than 3% of the population.) Scale bars, 10 μm.

		MIF2		mif2-2		mif2-3		cdc9		cdc16	
		23°	37°	23°	38°	23°	37°	23°	37°	23°	37°
% large budded cells		37	28	47	73	43	83	28	96	35	96
DNA	Spindle	% of cells with indicated morphologies									
		6	5	6	22	9	6	5	71	6	70
		2	2	6	31	26	34	2	21	4	23
		8	4	16	4	2	3	9	3	9	1
		<0.2	<0.2	0.4	10	2	34	0.3	<0.6	1	2
		19	15	19	2	3	2	9	<0.6	11	<0.6
		2	3	0.4	4	1	5	3	1	3	1

Figure 9. Spindle morphologies in large budded cells. Cells of the indicated genotypes were stained with DAPI and anti-tubulin antibodies for visualization of nuclear DNA and spindles at the permissive temperature and after 3 h at the restrictive temperature. The position of the nuclear DNA was scored as being in one of three classes: located at the mother-daughter neck and contained wholely within one cell body; extending across the mother-daughter neck; or separated into two discrete masses, one in each cell body. Spindles were classified as short and contained either in one cell body or extending across the neck; intermediate and extending across the neck; discontinuous with a non-staining area between the two SPBs, one in each cell body; elongated and continuous; or elongated and discontinuous. The percentage of total cells in the population in each class is given. Between 100 and 250 large budded cells were scored for each strain at both permissive and restrictive temperatures. Note that the percentages of each subclass do not add up exactly to the percentage of large budded cells in some columns due to rounding error. Strains used: *MIF2*, 5371-8-3; *mif2-2*, 6848-9-4; *mif2-3*, 6849-8-4; *cdc9*, 6898-3-2; *cdc16*, 6881-13-1.

had segregated into two discrete masses (Fig. 8 *F* and Fig. 9). In contrast, the majority of wild-type large budded cells had completed chromosome segregation. Furthermore, in *mif2* large budded cells at the restrictive temperature the chromosomal DNA was much less frequently located on one side of the neck (7% among *mif2-3* large budded cells) than extending across the neck (85% among *mif2-3* large budded cells) and sometimes appeared "stretched." Even at the permissive temperature the majority of *mif2-3* large budded cells contained DNA spanning the neck, suggesting a delay at this stage. For comparison, the G_2/early M phase arresting cell cycle mutants *cdc9* and *cdc16* were also examined. In contrast to *mif2*, of the large budded *cdc9* and *cdc16* cells having DNA located at or extending across the mother-daughter neck under restrictive conditions, the majority possessed nuclear DNA that was contained wholely within one cell body rather than extending across the neck (Fig. 9). A similar pattern has been observed in *cdc13*, *cdc20*, and *cdc23* (Palmer et al., 1989). In the less prevalent class of arrested *mif2* cells in which the nuclear DNA is situated at the mother-daughter neck but not extending across it, the DNA was located equally frequently in the mother and daughter, as determined by calcofluor staining. In contrast, in large budded wild-type cells having the nuclear DNA located at but not lying across the neck, the DNA was almost always located in the mother.

The distribution of spindle morphologies in *mif2* cells also differed greatly from wild-type (Fig. 9). The presence of short unelongated spindles in large budded cells is characteristic of cells blocked in S, G_2, or early M phase; this phenotype was observed in 53 and 40% of temperature arrested *mif2-2* and *mif2-3* cells, respectively (Fig. 8 *B* and Fig. 9). (Because *mif2* cells successfully complete DNA replication under restrictive conditions, we assume that these short spindle-containing cells are blocked in G_2 or early M.) In contrast, only 7–8% of wild-type cells were large budded and possessed similar short spindles; 18–21% of wild-type cells, however, contained fully elongated spindles, a class seen in only 6–7% of *mif2* cells under restrictive conditions (Fig. 8, *C* and *F*, and Fig. 9). For comparison, 92–93% of *cdc9* and *cdc16* cells contained short spindles at 37°C. We also observed a class of longer but not fully elongated spindles that was present only in cells in which the nuclear DNA spanned the mother-daughter neck (see diagram in Fig. 9). These intermediate length spindles were present in a greater proportion of wild-type large budded cells than in large budded *mif2* cells. The last class of spindle observed in *mif2* cells appeared discontinuous between the poles and was seen in 34% of temperature arrested *mif2-3* cells. In these cells, there was no tubulin staining in the central part of the spindle, as if the two half spindles had either failed to connect with or broken away from each other (Fig. 8, *A* and *B*). In some cases the two discontinuous halves were no longer arranged linearly, but at angles to the pole-to-pole axis (Fig. 8 *B*). This novel spindle morphology was also observed in temperature arrested *mif2-2* (14%, Fig. 9), *mif2-5* (10%), and *mif2-6* (18%) cells, but never in wild-type cells and only rarely in *cdc9* and *cdc16*.

To examine the discontinuous spindles in more detail, serial sections of temperature arrested *mif2*-3 cells were ex-

amined by electron microscopy. Each large budded cell contained a single nucleus and two SPBs embedded in the nuclear envelope. The structure of the SPBs and nuclear envelope appeared normal. Approximately half of the large budded cells contained spindles that appeared to have broken in half to form two short half spindles in which the spindle poles were no longer oriented parallel to one another (Fig. 10, *A* and *B*). Cytokinesis had not yet begun in these cells, indicating that broken spindles are not caused by cytokinesis through intact spindles. The remaining large budded cells contained short intact spindles, but as in the discontinuous spindles, the SPBs often appeared twisted away from each other instead of having a parallel alignment (Fig. 10 *C*) typical of wild-type short spindles. In these cells, intranuclear microtubules extending at angles to the main spindle axis were sometimes observed (Fig. 10 *C*). This stage is not observed in wild-type cells and may indicate an intermediate stage in loss of spindle continuity by *mif2* mutants. In the previously described lower resolution immunofluorescence studies, these aberrant continuous spindles were scored simply as intact short spindles resembling those of wild-type cells.

mif2 Spindles Break Apart during Anaphase Spindle Elongation

There are two points in the cell cycle at which discontinuous spindles might be likely to arise. First, discontinuous spindles could result if during spindle formation the SPBs begin to separate but fail to generate a continuous bipolar spindle between them. In *S. cerevisiae* spindle formation occurs before the completion of S phase, a point at which the bud is still significantly smaller than the mother. Second, spindles might break apart during spindle elongation as the two half spindles separate from each other in anaphase. At this stage, the size of the bud approaches that of the mother cell. To determine which of these two events gives rise to *mif2* discontinuous spindles, the time course of their appearance was monitored with respect to two other cell cycle markers, bud size and continuous short spindles. If discontinuous spindles result from a failure in spindle formation, then they should precede or coincide with the appearance of short spindles in the population, and appear in small budded cells. If *mif2* spindles fall apart due to defective anaphase spindle elongation, short spindles should indeed form, preceding the appearance of broken spindles in the population, and broken spindles should never appear in small budded cells. During exponential growth at 23°C, *mif2-3* cells were synchronized in G_1 by addition of α-factor. Arrested cells were shifted to 37°C, and the α-factor was removed. Spindle morphology, bud size, and viability were monitored at half hour intervals (Fig. 11). Short spindles first appeared at the 1 h timepoint and their proportion peaked at 1 1/2 h, the same time at which the proportion of short spindles peaked in a similarly treated wild-type culture. Discontinuous spindles did not appear until the 1 1/2 h timepoint and reached their highest level at 2 h. Small budded cells with discontinuous spindles were never observed. Furthermore, broken spindles appeared with similar kinetics to fully elongated mitotic spindles in wild-type cells (Fig. 11), suggesting that the elongated spindle morphology had been replaced by the broken spindle morphology in *mif2*. Therefore, *mif2* broken spindles likely result not from an inability to form spindles, but from a defect in anaphase spindle elongation. Alternatively, a lack of *MIF2* function may result in structurally defective spindles prone to breakage at the time of anaphase.

The fraction of cells with broken or breaking spindles at certain timepoints is underestimated in this experiment for two reasons. First, as was observed by electron microscopy, some spindles do not break completely and are therefore scored by immunofluorescence microscopy as intact short spindles. Furthermore, if spindles do indeed break but the two half spindles do not twist sufficiently from the central spindle axis in relation to the plane of observation, they will be scored as intact by immunofluorescence. Second, because *mif2* cells do not completely block progression through the cell cycle at the restrictive temperature (Fig. 5), cytokinesis of a cell containing a broken spindle could result in two unbudded daughter cells with one SPB each, which would be scored by immunofluorescence not as cells with broken spindles, but as unbudded G_1 cells. As a corollary to this idea, we reasoned that if cytokinesis occurred in cells stalled at the short spindle stage, in some cases an intact short spindle with two SPBs might be distributed to one cell and no spindle to the sister cell. A novel class of unbudded cells with complete short spindles representing up to 4% of the population does indeed arise at later timepoints, beginning at 2 h after the temperature shift.

We also measured the viability of *mif2* cells as they progressed through the cycle at 37°C (Fig. 11). Viability began to decline as *mif2* cells progressed through mitosis. The steepest drop in viability coincided with the period of greatest accumulation of broken spindles, which corresponds to the time of spindle elongation in wild-type cells. Although the curve specifying broken spindles begins to decline after the 2 h timepoint, viability continues to drop. If broken spindles and inviability are causally related, the increasing inviability may be due in part to greater numbers of broken spindles than are represented by the curve due to the underestimate of broken spindles (see above). However, there is clearly some inviability incurred at the short spindle stage, suggesting that the *MIF2* gene is required before the complete breaking apart of the spindle. The inviability observed at the short spindle stage may correspond to the initial stages of spindle breakage, which can be observed by electron microscopy but not by immunofluorescence microscopy.

Discussion

This work demonstrates that the *MIF2* gene is required for mitosis in *S. cerevisiae*. Mitotic defects result whether *MIF2* is overexpressed or deficient. When the *MIF2* gene was overexpressed, cells suffered increased missegregation of chromosomes during mitosis and a delay of the cell cycle in the G_2 and M phases. These defects suggest that *MIF2* contributes to the successful completion of a G_2/M event that is required for chromosome segregation and that is sensitive to the dosage of the proteins involved in its execution or regulation. Temperature sensitive alleles of *MIF2* arrested cell division primarily in early mitosis and displayed increased errors in chromosome segregation, supersensitivity to a microtubule destabilizing drug, inviability caused by passage through mitosis, and aberrant broken spindles, suggesting that *MIF2* is involved in spindle function. The lethality

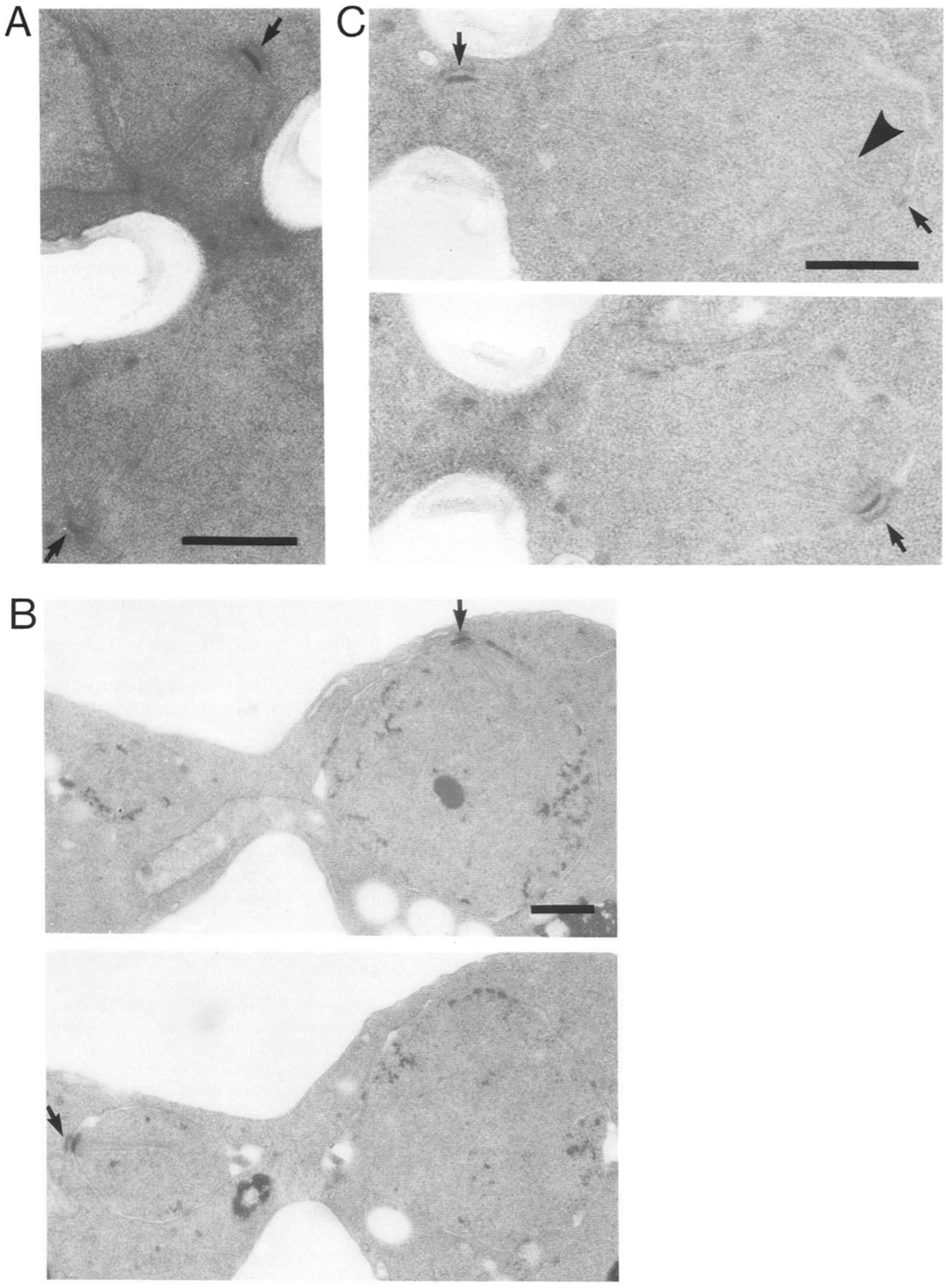
A
C
B

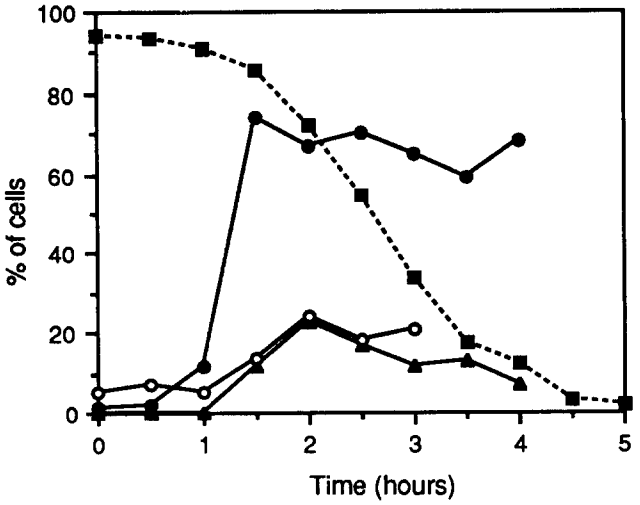

Figure 11. Kinetics of broken spindle appearance. The *mif2-3* strain 6849-10-1 was grown at 23°C to a cell density of 1.5 × 10^6 cells/ml in C medium, and then shifted to 37°C. Samples were removed at 1/2 h intervals, sonicated briefly to disperse cells, and diluted into −N medium. Part of each diluted sample was plated to C medium and grown to 23°C for determination of viability by the microcolony assay. Another part of each sample was prepared for immunofluorescence and examined for spindle morphology as described in Materials and Methods. Between 100 and 200 cells were scored by immunofluorescence for each data point. Also shown is the time course of appearance of elongated spindles in similarly treated wild-type cells (5371-10-2). ■: % viable *mif2* cells; ●: % *mif2* cells with short spindles; ▲: % *mif2* cells with broken spindles; ○: % wild-type cells with elongated spindles.

suffered by *mif2* mutants was accompanied by the appearance of the structurally aberrant spindles during mitosis. Broken spindles resulted when half spindles appeared to fall apart during unsuccessful anaphase spindle elongation.

The majority of temperature arrested *mif2* cells had one of two spindle types: a short spindle located at or across the neck of the bud that at first inspection appeared typical of spindles seen in G_2 or early M phase wild-type cells, or a broken spindle located across the neck. Closer examination of intact, short spindles by electron microscopy revealed that some appeared to be in an early stage of breaking apart, with the SPBs twisted away from each other and microtubules extending away from the central spindle axis. In cells containing either broken or intact spindles, the nuclear DNA was usually found spanning the mother-bud neck. Intact, short spindles also most frequently extended across the neck. This indicates that cytoplasmic microtubules, which are required for migration of the nucleus to the neck (Huffaker et al., 1988) and movement of the spindle through the neck into the daughter, are functional in cells deficient for *MIF2*. Both the preponderance of temperature arrested *mif2* cells with DNA spanning the mother-daughter neck as well as the frequent stretched appearance of the nuclear DNA as it extends across the neck differed from what was observed in wild-type cells and the G_2/early M mutants *cdc9* and *cdc16*. *mif2* mutants, therefore, may be blocked at a point in the cycle that is transient in wild-type cells—after movement of the nuclear DNA through the mother-bud neck but before completion of chromosome segregation—and that follows the *cdc9* and *cdc16* arrest points. Indeed, chromosomes may have already begun segregating at the *mif2* arrest point. Alternatively, the high frequency of DNA stretched across the neck in *mif2* cells may indicate that the nuclear DNA is in the process of transiting from one side of the neck to the other, as has been observed in temperature arrested *cdc16*, *cdc23*, *cdc13*, and *cdc17* strains, although at lower frequencies than in *mif2* (Palmer et al., 1989). *mif2* also resembles these *cdc* mutants in that when nuclear DNA is located solely on one side of the neck in arrested large budded cells, it is just as frequently located in the daughter as in the mother, indicating that nuclear DNA transits do occur. Nuclear transits may reflect a mechanism for movement of nuclear DNA, but whether they play a role in wild-type cells has not been determined.

Broken spindles, the second class of spindle most frequently seen in arrested *mif2* cells, were never observed in wild-type cells. *mif2* spindles apparently did not break during spindle assembly/formation nor by cytokinesis through an intact spindle. The broken spindle morphology rarely occurred in cells that had not moved the nuclear DNA through the mother-daughter neck, suggesting that breaks arise during anaphase/chromosome segregation. Kinetic experiments confirmed that spindles break apart during anaphase spindle elongation. A class of intermediate length or semi-elongated spindles present in wild-type large budded cells (Kilmartin and Adams, 1984) was infrequently observed in *mif2* cells at the restrictive temperature, suggesting that even this modest degree of spindle elongation may not be possible in the absence of *MIF2* function. Electron microscopic examination of broken spindles showed that they possess no spindle fibers running from pole to pole and that their SPBs face in random directions with respect to each other and remain separated, with one pole usually in the mother cell and one in the bud. This spindle morphology and arrangement of SPBs can be compared to those of the two other yeast mutants whose spindles break during anaphase, *espl* and *cin8 kipl*. The functionally redundant genes *CIN8* and *KIP1* encode putative kinesin-like microtubule motor proteins (Hoyt et al., 1992; Roof et al., 1992). In *cin8 kipl* double mutants, when *CIN8/KIP1* function is removed, short spindles lose structural integrity and the SPBs assume a side-by-side position (Saunders and Hoyt, 1992). SPBs undergo a similar fate when wild-type spindles are treated with the microtubule destabilizing drug nocodazole (Jacobs et al., 1988). As suggested by Saunders and Hoyt (1992), SPB collapse may indicate the loss of a force opposing another force that pulls the

Figure 10. Electron microscopy of temperature arrested *mif2* cells. *mif2-3* (6849-10-1) cells were grown to exponential phase at 23°C, shifted to 37°C for 3 1/3 h, and then fixed and prepared for electron microscopy. Because of the long distance between SPBs and their random orientation with respect to each other, it was rarely possible to find both SPBs in the same section. (*A*) A large budded cell containing a broken spindle. (*B*) Two serial sections through a cell showing a broken spindle. (*C*) Two serial sections through a cell showing an intact spindle whose SPBs are not oriented parallel to each other. Note the microtubules that have broken away from the central spindle (*arrowhead*). SPBs are indicated by arrows. Scale bars, 0.5 μm.

poles together. Interestingly, when *CIN8/KIP1* function is removed from spindles that have begun elongating or are fully elongated, no collapse is seen, suggesting an anaphase relaxation of the pole attracting force. Similarly, *mif2* spindles may not collapse because they have already entered anaphase. *espl* appears more similar to *mif2*: spindles lose continuity during elongation but do not immediately collapse to the side-by-side SPB formation (McGrew et al., 1992). Unlike *mif2*, however, *espl* preferentially segregates the chromosomal DNA and spindle into the daughter bud and continues additional cycles of SPB duplication and DNA replication after spindle breakage.

No extensive homologies were detected between the predicted Mif2 protein sequence and other protein sequences, but Mif2 did contain one subsequence resembling a motif required for binding of AT rich DNA by the *Drosophila* D1 and mammalian HMGI chromosomal proteins (Ashley et al., 1989; Reeves and Nissen, 1990). The HMGI DNA-binding domain has been shown to specifically contact six base or longer runs of A and T in the minor groove of double-stranded DNA (Solomon et al., 1986; Reeves and Nissen, 1990). HMGI has been immunolocalized to the AT rich G/Q bands and centromeric C bands of mammalian chromosomes (Disney et al., 1989). AT sequences within the repeated α-satellite DNA sequences found at all mammalian centromeres appear to specify the centromeric sites of HMGI binding (Strauss and Varshavsky, 1984). An attractive possibility is that the AT DNA-binding motif in the Mif2 protein allows binding to the centromere DNA element II of yeast centromeres, a 78–86-bp region composed of >90% A and T residues that are essential for both optimal centromere function in vivo (Fitzgerald-Hayes, 1987) and binding of minichromosome/protein complexes to microtubules in vitro (Kingsbury and Koshland, 1991). If Mif2 is a chromosomal protein, the extraordinarily acidic region located in the middle of the putative *MIF2* gene product may be important for contacting basic chromosomal proteins such as histones. The presence in the Mif2 sequence of several potential phosphorylation sites including one recognition determinant for Cdc28 protein kinase suggests that Mif2 activity may be regulated by phosphorylation. HMGI protein is an in vivo substrate for the mammalian homolog of the Cdc28 kinase, $p34^{cdc2}$, and is phosphorylated in a cell cycle-dependent manner (Lund and Layland, 1990; Reeves et al., 1991; Nissen et al., 1991). The site of phosphorylation is located immediately adjacent to the NH_2 terminus of one of the conserved AT DNA-binding domains. Phosphorylated peptides containing the DNA-binding domain have been shown to bind AT DNA in vitro with lower affinity than an unphosphorylated peptide (Reeves et al., 1991; Nissen et al., 1991). The Mif2 recognition determinant for Cdc28 kinase lies ~10 amino acids NH_2 terminal to the putative AT DNA-binding motif.

The breaking of spindles during anaphase suggests that *MIF2* is specifically required for maintenance of a rigid anaphase spindle. Broken spindles could be caused by defects in the processes of spindle elongation (anaphase B) or the separation and poleward movement of chromosomes (anaphase A). Alternatively, spindles might break due to structural instability that is manifested at the time of anaphase. During anaphase B, the overlapping anti-parallel microtubules of the two half spindles slide apart while simultaneously increasing their length by tubulin polymerization. Defects in either sliding or elongation might cause spindles to break. For example, using an in vitro model for anaphase B (Masuda and Cande, 1987), it was shown that diatom spindles break apart when sliding occurs in the absence of tubulin polymerization (Masuda et al., 1988). If Mif2 is a chromosomal protein, however, how might it function in anaphase B microtubule movements? Certain proteins from mammalian cells associate with chromosomes during prometaphase and metaphase but detach from chromosomes at the onset of anaphase and become localized to the spindle midzone, the site of anaphase B polar microtubule lengthening and sliding (for review see Earnshaw and Bernat, 1991). These "chromosomal passenger" proteins may use chromosomes simply as transportation to their site of action, suggesting one way that chromosomal proteins might contribute to the mechanics of spindle elongation.

Disruption of kinetochore microtubule function during anaphase A also could contribute to loss of spindle structural integrity. Before sister chromatid separation, opposing forces within the spindle act to balance each other, resulting in a stable spindle under tension (Nicklas and Koch, 1969; Nicklas, 1988; Goldstein, 1993). Poleward forces exerted by kinetochores on chromosomes may be balanced by the mechanical linkage between sisters as well as a pole-separating force caused by interactions among the anti-parallel polar microtubules. When the kinetochores of sisters separate, the tension is relaxed; chromosomes are translocated polewards and spindles elongate. If the tension were relaxed inappropriately in *mif2* mutants, for example due to defective connections between sisters, between kinetochores and centromeric DNA, or between kinetochores and microtubules, then broken spindles might result. For example, if connections between sisters were released before anaphase, an important contribution to spindle stability would be lost. If Mif2 is a chromosomal protein, then mutations in *MIF2* might render chromosomes poor substrates for interaction with the spindle or for segregation, perhaps by inefficient maintenance of the pole-sister-sister-pole tension within the spindle.

We thank J. Konopka, C. Mann, and the laboratory of B. Hall for vectors; R. Wickner and D. Hawthorne for strains; B. Garvik and T. Seeley for first noting the Mif2-D1 homology; B. Byers for advice; and J. McGrew for helpful discussions and comments on the manuscript.

This work was supported by a National Science Foundation graduate fellowship to M. T. Brown and by National Institutes of Health grants GM17709, GM18541, and GM07735. L. H. Hartwell was supported by an American Cancer Society research professor award.

Received for publication 4 November 1992 and in revised form 26 July 1993.

References

Ashley, C. T., C. G. Pendleton, W. W. Jennings, A. Saxena, and C. V. C. Glover. 1989. Isolation and sequencing of cDNA clones encoding *Drosophila* chromosomal protein D1. *J. Biol. Chem.* 264:8394–8401.

Baldari, C., and G. Cesareni. 1985. Plasmids pEMBLY: new single-stranded shuttle vectors for the recovery and analysis of yeast DNA sequences. *Gene (Amst.).* 35:27–32.

Baum, P., C. Yip, L. Goetsch, and B. Byers. 1988. A yeast gene essential for regulation of spindle pole duplication. *Mol. Cell. Biol.* 8:5386–5397.

Beach, D., L. Rodgers, and J. Gould. 1988. *RAN1*$^+$ controls the transition from mitotic division to meiosis in fission yeast. *Curr. Genet.* 10:297–311.

Belfort, M., and J. Pedersen-Lane. 1984. Genetic system for analyzing *Escherichia coli* thymidylate synthase. *J. Bacteriol.* 160:371–378.

Boeke, J. D., F. Lacroute, and G. R. Fink. 1984. A positive selection for mutants lacking orotidine 5'-phosphate decarboxylase activity in yeast: 5-fluoroorotic acid resistance. *Mol. & Gen. Genet.* 181:288–291.

Broach, J. R., J. N. Strathern, and J. B. Hicks. 1979. Transformation in yeast: development of a hybrid cloning vector and isolation of the *CAN1* gene. *Gene (Amst.).* 8:121–133.

Brown, M., T. Formosa, L. Hartwell, L. Kadyk, and T. Weinert. 1993. Analysis of the *S. cerevisiae* nuclear cycle. *In* Molecular Biology of the Yeast *Saccharomyces*. vol. 3. J. R. Broach, J. R. Pringle, and E. W. Jones, editors. Cold Spring Harbor Laboratory Press, Cold Spring Harbor, NY.

Brutlag, D. L., J.-P. Dautricourt, S. Maulik, and J. Relph. 1990. Improved sensitivity of biological sequence database searches. *Comp. App. Biol. Sci.* 6:237–245.

Byers, B., and L. Goetsch. 1975. The behavior of spindles and spindle plaques in the cell cycle and conjugation of *Saccharomyces cerevisiae*. *J. Bacteriol.* 124:511–523.

Byers, B., and L. Goetsch. 1991. Preparation of yeast cells for thin-section electron microscopy. *Methods Enzymol.* 194:602–608.

Cande, W. Z., and C. J. Hogan. 1989. The mechanism of anaphase spindle elongation. *BioEssays.* 11:5–9.

Chu, G., D. Vollrath, and R. W. Davis. 1986. Separation of large DNA molecules by contour-clamped homogeneous electric fields. *Science (Wash. DC).* 234:1582–1585.

Clarke, L., and J. Carbon. 1980. Isolation of a yeast centromere and construction of functional small circular chromosomes. *Nature (Lond.).* 287: 504–509.

Cross, F. R. 1988. *DAF1*, a mutant gene affecting size control, pheromone arrest, and cell cycle kinetics of *Saccharomyces cerevisiae*. *Mol. Cell. Biol.* 8:4675–4684.

Disney, J. E., K. R. Johnson, N. S. Magnuson, S. R. Sylvester, and R. Reeves. 1989. High-mobility group protein HMGI localizes to G/Q- and C-bands of human and mouse chromosomes. *J. Cell Biol.* 109:1975–1982.

Doolittle, R. F. 1986. Of URFs and ORFs: a primer on how to analyze derived amino acid sequences. University Science Books, Mill Valley, CA. 103 pp.

Earnshaw, W. C., and R. L. Bernat. 1991. Chromosomal passengers: toward an integrated view of mitosis. *Chromosoma (Berl.).* 100:139–146.

Fitzgerald-Hayes, M. 1987. Yeast centromeres. *Yeast.* 3:187–200.

Goldstein, L. S. B. 1993. Functional redundancy in mitotic force generation. *J. Cell Biol.* 120:1–3.

Hartwell, L. H. 1967. Macromolecular synthesis in temperature-sensitive mutants of yeast. *J. Bacteriol.* 93:1662–1670.

Hartwell, L. H., and D. Smith. 1985. Altered fidelity of mitotic chromosome transmission in cell cycle mutants of *S. cerevisiae*. *Genetics.* 110:381–395.

Hartwell, L. H., and T. A. Weinert. 1989. Checkpoints: controls that ensure the order of cell cycle events. *Science (Wash. DC).* 246:629–634.

Henikoff, S. 1984. Unidirectional digestion with exonuclease III creates targeted breakpoints for DNA sequencing. *Gene (Amst.).* 28:351–359.

Hoyt, M. A., L. He, K. K. Loo, and W. S. Saunders. 1992. Two *Saccharomyces cerevisiae* kinesin-related gene products required for mitotic spindle assembly. *J. Cell Biol.* 118:109–120.

Huffaker, T. C., J. H. Thomas, and D. Botstein. 1988. Diverse effects of β-tubulin mutations on microtubule formation and function. *J. Cell Biol.* 106: 1997–2010.

Hutter, K. J., and H. E. Eipel. 1979. Microbial determination by flow cytometry. *J. Gen. Microbiol.* 113:369–375.

Jacobs, C. W., A. E. M. Adams, P. J. Szaniszlo, and J. R. Pringle. 1988. Functions of microtubules in the *Saccharomyces cerevisiae* cell cycle. *J. Cell Biol.* 107:1409–1426.

Johnson, K. R., D. A. Lehn, T. S. Elton, P. J. Barr, and R. Reeves. 1988. Complete murine cDNA sequence, genomic structure, and tissue expression of the high mobility group protein HMG-I (Y). *J. Biol. Chem.* 263: 18338–18342.

Johnson, K. R., D. A. Lehn, and R. Reeves. 1989. Alternative processing of mRNAs encoding mammalian chromosomal high-mobility-group proteins HMGI and HMGY. *Mol. Cell Biol.* 9:2114–2123.

Johnston, G. C., J. R. Pringle, and L. H. Hartwell. 1977. Coordination of growth with cell division in the yeast *Saccharomyces cerevisiae*. *Exp. Cell Res.* 105:79–98.

Kennelly, P. J., and E. G. Krebs. 1991. Consensus sequences as substrate specificity determinants for protein kinases and protein phosphatases. *J. Biol. Chem.* 266:15555–15558.

Kilmartin, J. V., and A. E. M. Adams. 1984. Structural rearrangements of tubulin and actin during the cell cycle of the yeast *Saccharomyces*. *J. Cell Biol.* 98:922–933.

Kilmartin, J. V., B. Wright, and C. Milstein. 1982. Rat monoclonal antitubulin antibodies derived by using a new non-secreting rat cell line. *J. Cell Biol.* 93:576–582.

Kingsbury, J., and D. Koshland. 1991. Centromere-dependent binding of yeast minichromosomes to microtubules *in vitro*. *Cell* 66:483–495.

Koshland, D., J. C. Kent, and L. H. Hartwell. 1985. Genetic analysis of the mitotic transmission of minichromosomes. *Cell.* 40:393–403.

Kozak, M. 1984. Compilation and analysis of sequences upstream from the translational start site in eukaryotic mRNAs. *Nucleic Acids Res.* 12: 857–872.

Lea, D. E., and C. A. Coulson. 1949. The distribution of numbers of mutants in bacterial populations. *J. Genet.* 49:264–284.

Levinger, L., and A. Varshavsky. 1982. Protein D1 preferentially binds (A+T)-rich DNA *in vitro* and is a component of *Drosophila melanogaster* nucleosomes containing (A+T)-rich satellite DNA. *Proc. Natl. Acad. Sci. USA.* 79:7152–7156.

Lund, T., and S. G. Layland. 1990. The metaphase specific phosphorylation of HMGI. *Biochem. Biophys. Res. Commun.* 171:342-347.

Lund, T., K. H. Dahl, E. Mork, J. Holtlund, and S. G. Laland. 1987. The human chromosomal protein HMGI contains two identical palindrome amino acid sequences. *Biochem. Biophys. Res. Commun.* 146:725–730.

Mann, C., J.-M. Buhler, I. Treich, and A. Sentenac. 1987. *RPC40*, a unique gene for a subunit shared between yeast RNA polymerases A and C. *Cell.* 48:627–637.

Masuda, H., and W. Z. Cande. 1987. The role of tubulin polymerization during spindle elongation *in vitro*. *Cell.* 49:193–202.

Masuda, H., K. L. McDonald, and W. Z. Cande. 1988. The mechanism of anaphase spindle elongation: uncoupling of tubulin incorporation and microtubule sliding during *in vitro* spindle reactivation. *J. Cell Biol.* 107: 623–633.

McGrew, J. T., L. Goetsch, B. Byers, and P. Baum. 1992. Requirement for *ESP1* in the nuclear division cycle of *Saccharomyces cerevisiae*. *Mol. Biol. Cell.* 3:1443–1454.

McIntosh, J. R., and M. P. Koonce. 1989. Mitosis. *Science (Wash. DC).* 246:622–628.

Meeks-Wagner, D., and L. H. Hartwell. 1986. Normal stoichiometry of histone dimer sets is necessary for high fidelity of mitotic chromosome transmission. *Cell.* 44:43–52.

Meeks-Wagner, D., J. S. Wood, B. Garvik, and L. H. Hartwell. 1986. Isolation of two genes that affect mitotic chromosome transmission in *S. cerevisiae*. *Cell.* 44:53–63.

Moreno, S., and P. Nurse. 1990. In vivo veritas? *Cell.* 61:549–551.

Mortimer, R. K., and D. Schild. 1985. Genetic map of *Saccharomyces cerevisiae*. 9th Ed. *Microbiol. Rev.* 49:181–212.

Nicklas, R. B. 1988. The forces that move chromosomes in mitosis. *Annu. Rev. Biophys. Biophys. Chem.* 17:431–449.

Nicklas, R. B., and C. A. Koch. 1969. Chromosome micromanipulation: spindle fiber tension and the reorientation of mal-oriented chromosomes. *J. Cell Biol.* 43:40–50.

Nissen, M. S., T. A. Langan, and R. Reeves. 1991. Phosphorylation by cdc2 kinase modulates DNA binding activity of high mobility group I nonhistone chromatin protein. *J. Biol. Chem.* 266:19945–19952.

Palmer, R. E., M. Koval, and D. Koshland. 1989. The dynamics of chromosome movement in the budding yeast *Saccharomyces cerevisiae*. *J. Cell Biol.* 109:3355–3366.

Perkins, D. D. 1979. Biochemical mutants in the smut fungus *Ustilago maydis*. *Genetics.* 34:607–626.

Reeves, R., and M. S. Nissen. 1990. The AT-DNA-binding domain of mammalian high mobility group I chromosomal proteins. *J. Biol. Chem.* 265: 8573–8582.

Reeves, R., T. A. Langan, and M. S. Nissen. 1991. Phosphorylation of the DNA-binding domain of nonhistone high-mobility group I protein by cdc2 kinase: reduction of binding affinity. *Proc. Natl. Acad. Sci. USA.* 88: 1671–1675.

Roof, D. M., P. B. Meluh, and M. D. Rose. 1992. Kinesin-related proteins required for assembly of the mitotic spindle. *J. Cell Biol.* 118:95–108.

Rose, M. D., and G. R. Fink. 1987. *KAR1*, a gene required for function of both intranuclear and extranuclear microtubules in yeast. *Cell.* 48:1047–1060.

Sanger, F., S. Nicklen, and A. R. Coulson. 1977. DNA sequencing with chain-terminating inhibitors. *Proc. Natl. Acad. Sci. USA.* 82:5463–5467.

Saunders, W. S., and M. A. Hoyt. 1992. Kinesin-related proteins required for structural integrity of the mitotic spindle. *Cell.* 70:451–458.

Schatz, P. J., F. Solomon, and D. Botstein. 1988. Isolation and characterization of conditional-lethal mutations in the *TUB1* α-tubulin gene of the yeast *Saccharomyces cerevisiae*. *Genetics.* 120:681–695.

Scherer, S., and R. W. Davis. 1979. Replacement of chromosome segments with altered DNA sequences constructed *in vitro*. *Proc. Natl. Acad. Sci. USA.* 76:4951–4955.

Sclafani, R. F., and W. L. Fangman. 1984. Conservative replication of double-stranded RNA in *Saccharomyces cerevisiae* by displacement of progeny single strands. *Mol. Cell. Biol.* 4:1618–1626.

Sharp, P. M., and W.-H. Li. 1987. The codon adaptation index—a measure of directional synonymous codon usage bias, and its potential applications. *Nucleic Acids Res.* 15:1281–1295.

Sherman, G., G. R. Fink, and J. B. Hicks. 1986. Methods in Yeast Genetics. Cold Spring Harbor Laboratory Press, Cold Spring Harbor, NY. 186 pp.

Solomon, M. J., F. Strauss, and A. Varshavsky. 1986. A mammalian high mobility group protein recognizes any stretch of six AT base pairs in duplex DNA. *Proc. Natl. Acad. Sci. USA.* 83:1276–1280.

Strauss, F., and A. Varshavsky. 1984. A protein binds to a satellite DNA repeat at three specific sites that would be brought into mutual proximity by DNA folding in the nucleosome. *Cell.* 37:889–901.

Struhl, K., D. T. Stinchcomb, S. Scherer, and R. W. Davis. 1979. High frequency transformation of yeast: autonomous replication of hybrid DNA molecules. *Proc. Natl. Acad. Sci. USA.* 76:1035–1039.

Thomas, J. H., N. F. Neff, and D. Botstein. 1985. Isolation and characterization of mutations in the β-tubulin gene of *Saccharomyces cerevisiae*. *Genetics.* 112:715–734.

Tschumper, G., and J. Carbon. 1980. Sequence of a yeast DNA fragment containing a chromosomal replicator and the *TRP1* gene. *Gene (Amst.).* 10: 157–166.

Weinert, T. A., and L. H. Hartwell. 1988. The *RAD9* gene controls the cell cycle response to DNA damage in *Saccharomyces cerevisiae*. *Science (Wash. DC).* 241:317–322.

Weinert, T. A., and L. H. Hartwell. 1993. Cell cycle arrest of *cdc* mutants and specificity of the *RAD9* checkpoint. *Genetics.* 134:63–80.